



This is a repository copy of *Adipose-derived stem cells protect motor neurons and reduce glial activation in both in vitro and in vivo models of ALS.*

White Rose Research Online URL for this paper:
<http://eprints.whiterose.ac.uk/173126/>

Version: Published Version

Article:

Ciervo, Y., Gatto, N., Allen, C. et al. (4 more authors) (2021) Adipose-derived stem cells protect motor neurons and reduce glial activation in both in vitro and in vivo models of ALS. *Molecular Therapy — Methods & Clinical Development*, 21. pp. 413-433. ISSN 2329-0501

<https://doi.org/10.1016/j.omtm.2021.03.017>

Reuse

This article is distributed under the terms of the Creative Commons Attribution-NonCommercial-NoDerivs (CC BY-NC-ND) licence. This licence only allows you to download this work and share it with others as long as you credit the authors, but you can't change the article in any way or use it commercially. More information and the full terms of the licence here: <https://creativecommons.org/licenses/>

Takedown

If you consider content in White Rose Research Online to be in breach of UK law, please notify us by emailing eprints@whiterose.ac.uk including the URL of the record and the reason for the withdrawal request.



eprints@whiterose.ac.uk
<https://eprints.whiterose.ac.uk/>

Adipose-derived stem cells protect motor neurons and reduce glial activation in both *in vitro* and *in vivo* models of ALS

Yuri Ciervo,¹ Noemi Gatto,¹ Chloe Allen,¹ Andrew Grierson,¹ Laura Ferraiuolo,¹ Richard J. Mead,^{1,2} and Pamela J. Shaw^{1,2}

¹Sheffield Institute for Translational Neuroscience (SITraN), Department of Neuroscience, Faculty of Medicine, Dentistry and Health, The University of Sheffield, 385 Glossop Rd., Sheffield S10 2HQ, UK

Amyotrophic lateral sclerosis (ALS) is a devastating neurodegenerative condition for which new therapeutic options are urgently needed. We injected GFP⁺ adipose-derived stem cells (EGFP-ADSCs) directly into the cerebrospinal fluid (CSF) of transgenic SOD1^{G93A} mice, a well-characterized model of familial ALS. Despite short-term survival of the injected cells and limited engraftment efficiency, EGFP-ADSCs improved motor function and delayed disease onset by promoting motor neuron (MN) survival and reducing glial activation. We then tested the *in vitro* neuroprotective potential of mouse ADSCs in astrocyte/MN co-cultures where ALS astrocytes show neurotoxicity. ADSCs were able to rescue MN death caused by ALS astrocytes derived from symptomatic SOD1^{G93A} mice. Further, ADSCs were found to reduce the inflammatory signature of ALS astrocytes by inhibiting the release of pro-inflammatory mediators and inducing the secretion of neuroprotective factors. Finally, mouse ADSCs were able to protect MNs from the neurotoxicity mediated by human induced astrocytes (iAstrocytes) derived from patients with either sporadic or familial ALS, thus for the first time showing the potential therapeutic translation of ADSCs across the spectrum of human ALS. These data in two translational models of ALS show that, through paracrine mechanisms, ADSCs support MN survival and modulate the toxic microenvironment that contributes to neurodegeneration in ALS.

INTRODUCTION

Amyotrophic lateral sclerosis (ALS) is a devastating neurodegenerative condition characterized by the selective loss of both upper and lower motor neurons (MNs) leading to muscle denervation, paralysis, and ultimately death within 2–5 years from diagnosis.¹ ALS is mainly sporadic (sALS) in origin, but familial forms of the disease (fALS) account for ~10% of cases.² Mutations in the superoxide dismutase 1 (SOD1) gene are responsible for 15%–20% of fALS.³ Transgenic mice expressing a high copy number of the human SOD1 gene harboring the G93A mutation (SOD1^{G93A}) recapitulate several clinical and pathological features seen in the human disease and represent a validated and robust model to investigate new therapeutic strate-

gies.^{4,5} ALS is a multifactorial disease where several impaired molecular mechanisms are involved, including mitochondrial dysfunction, protein mis-localization and aggregation, glutamate excitotoxicity, impaired axonal transport, oxidative stress, and dysregulation of RNA processing.^{6–9} Moreover, damage to MNs and disease progression are strongly amplified by dysfunction and aberrant activation of non-neuronal cells such as astrocytes and microglia.^{10–12} Because of the complexity and non-cell-autonomous nature of the disease, therapeutic approaches targeting multiple mechanisms have been proposed to be beneficial in ALS.^{13,14}

The use of stem cells as a therapeutic tool for ALS is a therapeutic approach with potential for targeting multiple disease mechanisms.¹⁵ Mesenchymal stem cells (MSCs) can be obtained from adults, show low immunogenicity, and can target multiple disease pathways through immunomodulation and secretion of trophic factors, cytokines, and exosomes.¹⁴ In several studies, MSCs transplanted intravenously, intraparenchymally, intrathecally, or intramuscularly were able to ameliorate the phenotype of SOD1^{G93A} rodents by improving motor function, reducing neuroinflammation, slowing disease progression, and extending lifespan.¹⁴ Since the therapeutic effects of MSCs seem to be mediated through paracrine effects rather than cell replacement, direct delivery of cells into the cerebrospinal fluid (CSF) may provide the safest and most efficacious delivery route in order to modulate the toxic environment leading to motor neuron degeneration.^{16–20} For several years, bone marrow aspirates have been considered the reference source for MSCs (BM-MSCs).

Received 1 March 2021; accepted 23 March 2021;

<https://doi.org/10.1016/j.omtm.2021.03.017>.

²Senior author

Correspondence: Pamela J. Shaw, Professor, Dame, Sheffield Institute for Translational Neuroscience (SITraN), Department of Neuroscience, Faculty of Medicine, Dentistry and Health, The University of Sheffield, 385 Glossop Rd., Sheffield S10 2HQ, UK.

E-mail: pamela.shaw@sheffield.ac.uk

Correspondence: Richard J. Mead, PhD, Sheffield Institute for Translational Neuroscience (SITraN), Department of Neuroscience, Faculty of Medicine, Dentistry and Health, The University of Sheffield, 385 Glossop Rd., Sheffield S10 2HQ, UK.

E-mail: r.j.mead@sheffield.ac.uk



However, bone marrow aspiration is expensive and invasive and gives rise to a limited number of stem cells.²¹ Adipose tissue may represent a valid alternative source of MSCs for clinical application.^{22,23} Indeed, adipose-derived stem cells (ADSCs) can be harvested through a less invasive procedure such as liposuction, are more abundant, and show greater *ex vivo* proliferative capacity and a lower senescence ratio compared with BM-MSCs.^{24–27}

In the present study, we investigated the therapeutic potential of mouse-derived ADSCs in both *in vivo* and *in vitro* models of ALS. First, we tested the efficacy of intrathecal transplantation of ADSCs in pre-symptomatic SOD1^{G93A} mice of the defined C57BL/6J genetic background by evaluating motor performance, disease onset, and CNS pathology. We also monitored the survival, engraftment, and distribution of ADSCs over time by histological analysis. In the second part of the study, we tested the neuroprotective potential of ADSCs in astrocyte/MN co-cultures where ALS astrocytes (derived from either SOD1^{G93A} mice or human ALS patients) show neurotoxicity.^{28–30} We then explored the immunomodulatory potential of ADSCs *in vitro* by evaluating the secretion of pro-inflammatory mediators and growth factors from SOD1^{G93A} mouse astrocytes, utilizing separated co-cultures. Our data in two translational models of ALS indicate that the therapeutic potential of ADSCs is mediated by the release of soluble factors able to directly and indirectly support MN survival and reduce neuroinflammation.

RESULTS

Characterization of mouse adipose-derived stem cells

Mouse ADSCs (mADSCs) were isolated from the inguinal fat pads of healthy 8- to 10-week-old non-transgenic (NTg) C57BL/6 mice, expanded *in vitro* for 5 passages, and phenotypically and functionally characterized as previously described.³¹ The immunophenotype of ADSCs was determined by flow cytometry. ADSCs expressed the mesenchymal stem cell surface markers (CD44, CD90, CD29, CD106, and CD105) but were negative for CD73 and endothelial (CD31) and hematopoietic (CD34, CD11b, CD45) markers (Figure 1A). A tri-lineage differentiation assay confirmed the multipotential differentiation capability of ADSCs (Figure 1B).

Transplanted EGFP-ADSCs engraft and survive in the subarachnoid space of SOD1^{G93A} mice

To monitor *in vivo* biodistribution, ADSCs were infected with lentivirus encoding enhanced green fluorescent protein (EGFP). Fluorescent microscopy and flow cytometry showed high transduction efficiency (>98%) and robust expression of EGFP (Figures S1A and S1B). To exclude alteration of cell characteristics following integration of EGFP into the genome, EGFP-ADSCs were subjected to phenotypic and functional analysis as before, indicating no change in either surface marker expression or differentiation capacity (Figures S2A and S2B).

In order to achieve both brain and spinal cord distribution of ADSCs in transplanted mice, 5×10^5 EGFP-ADSCs were injected directly into the CSF of 30-day-old SOD1^{G93A} mice via the cisterna magna. Cell

dosage was chosen based on the literature^{18,32} and on pilot studies (data not shown). To evaluate engraftment and survival of the injected EGFP-ADSCs, mice were sacrificed 7-, 14-, 21-, and 28-days post-transplantation ($n = 3$ per group). In order to preserve the meninges and allow detection of cells within the subarachnoid space, the brain and spinal cord were processed and carefully dissected with intact dura mater as previously described.³² At 1 week post-injection, most of the detected cells were found in clusters close to the site of injection (cisterna magna) and in the IV ventricle (Figure 2A). Clusters of GFP⁺ cells were also found around the brainstem (cisterna pontine) (Figure 2B) and lateral recesses (Figure 2C) and along the spinal cord (at cervical, thoracic, and lumbar levels) confined to the subarachnoid space (Figure 2D). Two weeks after injection, EGFP-ADSCs were still detected in the IV ventricle (Figure 2E), cisterna pontine (Figure 2F), and lateral recesses close to the choroid plexus (Figure 2G), where occasionally cells were found to migrate into the brainstem. Interestingly, ADSCs that survived in the subarachnoid space of the spinal cord migrated toward both dorsal and ventral root ganglia (Figure 2H); however, no cells have penetrated. Three weeks post-transplantation, the survival of EGFP-ADSCs within the IV ventricle and cisterna pontine decreased considerably (Figures 2I and 2J), while clusters of GFP⁺ cells persisted in the lateral recesses (Figure 2K). Cells were still detected in the subarachnoid space of the spinal cord (Figure 2L). At week 4, very few EGFP-ADSCs were found to survive within the ventricular system and were confined to the spinal cord meninges (Figures 2M–2P). No fluorescent signal was detected in control phosphate-buffered saline (PBS)-injected mice (Figures 2Q–2T).

Intrathecal injection of EGFP-ADSCs improves motor function and delays disease onset in SOD1^{G93A} mice

We next investigated whether intrathecal transplantation of EGFP-ADSCs into pre-symptomatic transgenic SOD1^{G93A} mice could delay motor function decline and the onset of visible signs of disease as a proof of concept for therapeutic intervention. In our congenic strain of transgenic SOD1^{G93A} mice, a significant decline in motor function is detectable by rotarod as early as 40 days of age before visible signs of the disease are detected.³³ This allows the design of a relatively short protocol for preclinical therapeutic investigation (Figure 3A). Mice between 30 and 32 days of age were randomly assigned to the EGFP-ADSC treatment (5×10^5 EGFP-ADSCs, $n = 15$) or vehicle (PBS, $n = 15$) group. To evenly distribute the parentage, litters were matched between treatment groups. ADSC-injected mice showed a significant increase in body weight compared with the vehicle group from 60 days of age, which persisted until the end of the study (PBS-injected mice 16.0 g (± 0.8 SD) at 90 days versus EGFP-ADSC-injected mice 17.5 g (± 0.9 SD), overall treatment effect of $p < 0.0001$, 2-way ANOVA; $p = 0.0012$ at 90 days, Bonferroni post-test; Figure 3B). Stem cell-transplanted mice performed better on the rotarod task throughout the study compared with PBS-injected mice (overall treatment effect of $p = 0.039$, 2-way ANOVA; Figure 3C). Motor performance decline, measured as 20% reduction from peak of performance,³³ was significantly delayed in ADSC-transplanted mice by ~ 2 weeks (PBS-injected mice 7.4 weeks (± 2.0 SD) versus EGFP-ADSC injected mice 9.3 weeks (± 2.3 SD), $p = 0.026$, Mann-Whitney test; Figure 3D). Onset of visible signs of disease

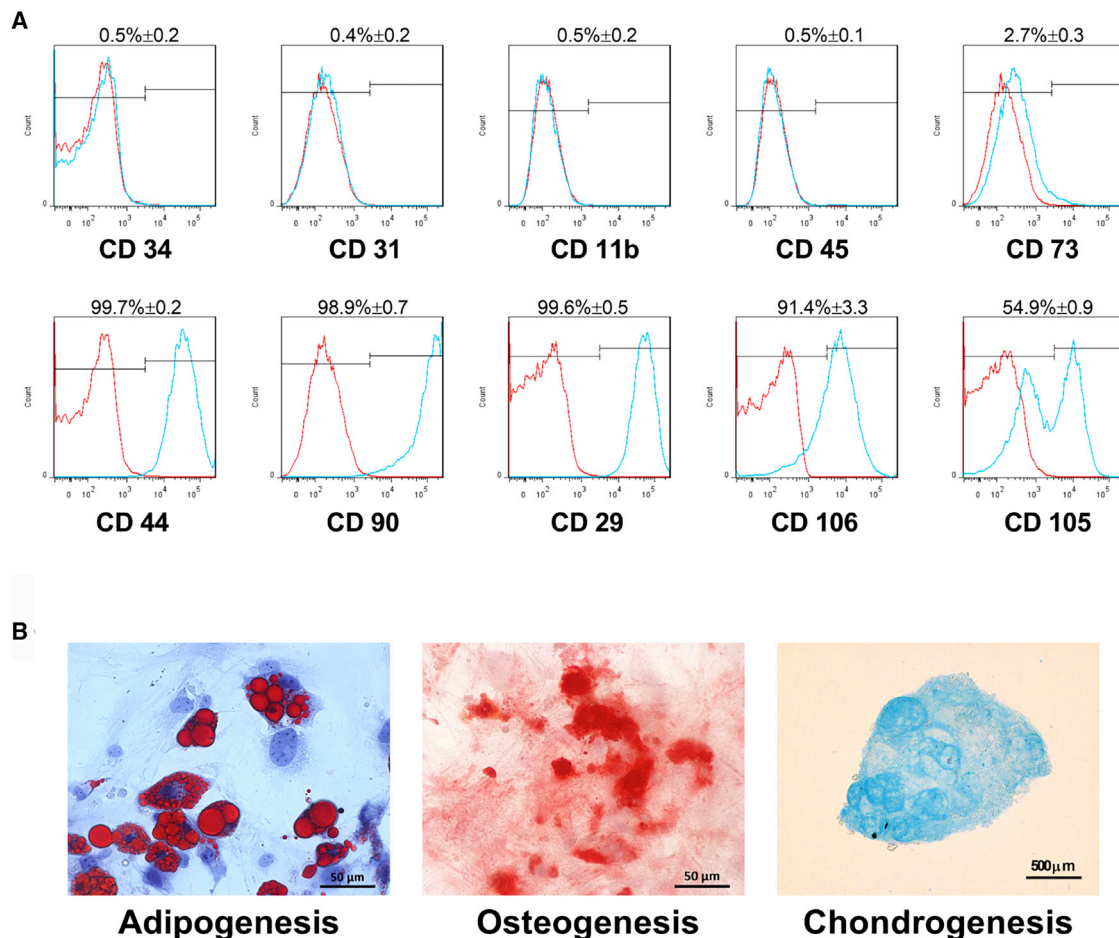


Figure 1. Isolated mADSCs display the expected surface markers and tri-lineage differentiation capacity

ADSCs were isolated from mouse inguinal fat pads and expanded *in vitro*. Immunophenotyping and differentiation capacity were evaluated to confirm their identity. (A) Immunophenotype of mADSCs at passage 5 by flow cytometry analysis. The histogram in blue represents the cells stained with the specific antibody, and in red is represented the staining with the isotype-matched control antibody. On the abscissa is indicated the fluorescence intensity and on the ordinate the cell counts. The percentage of positive cells is relative to the intensity of the isotype controls. mADSCs were negative (<0.5%) for the hematopoietic and endothelial markers CD34, CD31, CD11b, and CD45, while CD73 was expressed in <3% of the total cell population. Notably, mADSCs were positive (>90%) for the MSC markers CD44, CD90, CD29, and CD106. The expression of CD105 was detected in ~54% of mADSCs. Percentage values represent average from 3 independent experiments \pm SD. (B) Tri-lineage differentiation of mADSCs after exposure to specific induction media (see [Materials and methods](#)). From left to right, adipogenesis was confirmed by oil red O staining, osteogenesis by alizarin red O staining, and chondrogenesis by Alcian blue staining. Images are representative of at least 3 independent experiments.

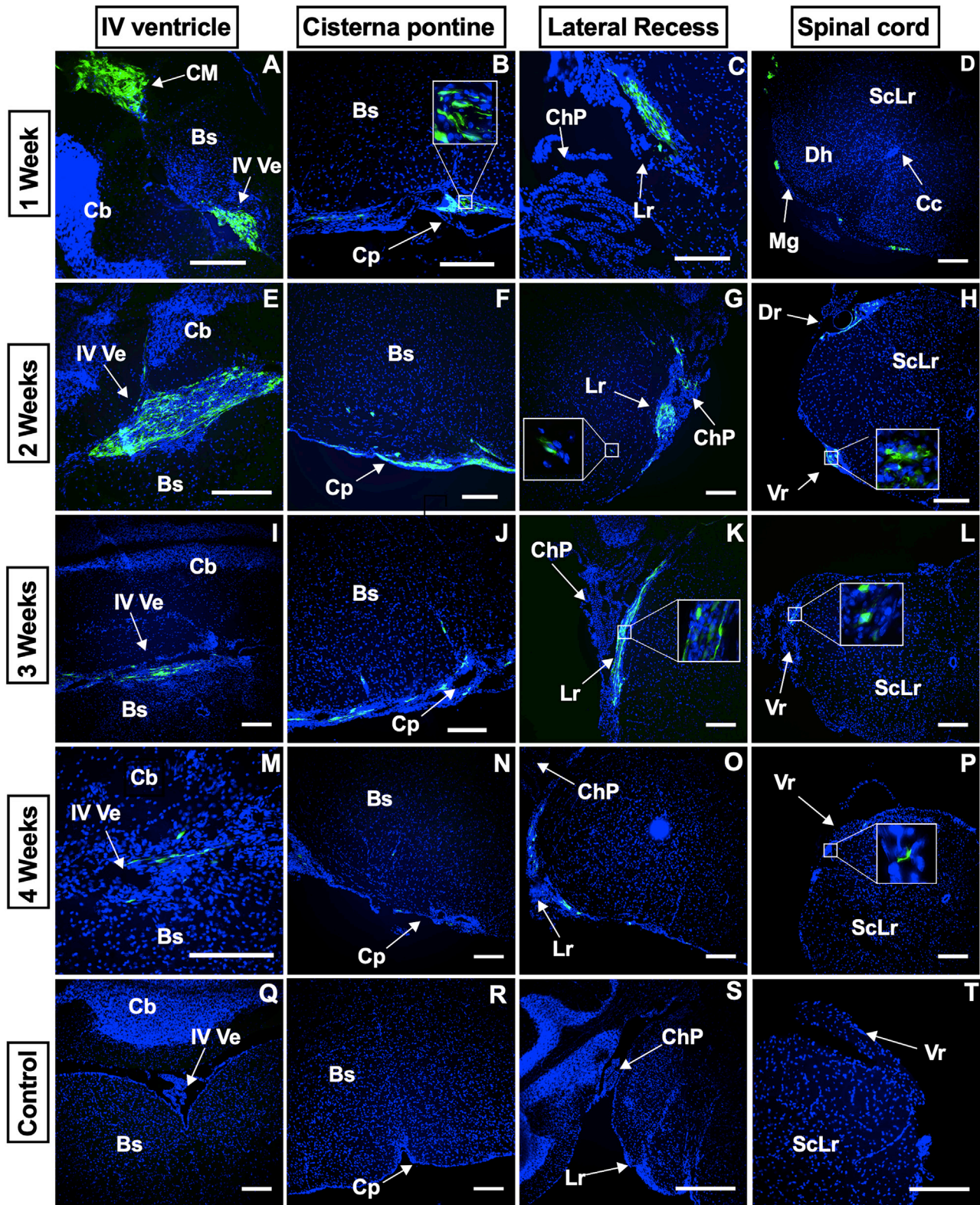
defined by hindlimb splay defect plus tremor was also delayed by 5 days in ADSC-injected mice compared with controls (PBS-injected mice 68.1 days (\pm 4 SD) versus EGFP-ADSC-injected mice 73.5 days (\pm 3.5 SD), $p = 0.0005$, unpaired *t* test; [Figure 3E](#)). We performed CatWalk gait analysis at time points previously identified as informative of motor impairment³³ (days 70 and 84, $n = 5$ /group). ADSC-treated mice showed significant improvements in gait parameters compared with the vehicle group ([Figure S3](#)).

Intrathecal injection of ADSCs protects motor neurons and reduces glial activation in SOD1^{G93A} mice

To investigate whether the therapeutic effects noted above result from protection of MNs, we performed Nissl staining on lumbar spinal

cord sections obtained from 90-day-old mice ($n = 6$ per group) and counted large MNs within the ventral horn. ADSC-injected mice had significantly more MNs compared with the PBS-injected control group (PBS-injected mice 2.5 MNs (\pm 0.2 SD) per ventral horn (10- μ m-thickness sections) versus EGFP-ADSC injected mice 3.1 MNs (\pm 0.4 SD) per ventral horn, $p = 0.0434$, 1-way ANOVA with Tukey's test; [Figures 4A and 4B](#)).

There is evidence that MN death in ALS could result from aberrant glial activation, which in itself is a hallmark of disease progression in ALS.¹² To determine whether this may be a relevant mechanism in the ADSC therapeutic effect, we performed immunohistochemistry on the lumbar enlargement of the spinal cord of 90-day-old mice to



(legend on next page)

evaluate astrogliosis (glial fibrillary acidic protein [GFAP] staining) and microgliosis (Iba-1 staining). Astrocyte activation, evaluated by GFAP total staining area, was significantly reduced in ADSC-treated mice compared with vehicle-treated mice (PBS-injected mice $7,191 \mu\text{m}^2$ (± 634 SD) versus EGFP-ADSC-injected mice $6,203 \mu\text{m}^2$ (± 774 SD) (10- μm -thickness sections), $n = 6/\text{group}$, $p = 0.0413$, 1-way ANOVA with Tukey's test; **Figures 4A and 4B**; **Figures S4A and S4B**). Microglial activation, defined by IBA-1 total staining area, was also significantly attenuated in ADSC-recipient mice compared with control mice (PBS-injected mice $2,921 \mu\text{m}^2$ (± 154 SD) versus EGFP-ADSC-injected mice $2,075 \mu\text{m}^2$ (± 67 SD) (10- μm -thickness sections), $n = 6/\text{group}$, $p < 0.0001$, 1-way ANOVA with Tukey's test; **Figures 4C and 4D**; **Figures S4A and S4B**). These results are in agreement with a beneficial clinical effect on MN survival associated with a reduction in the spinal cord inflammatory milieu mediated by astrocyte and microglial activation.

ADSCs protect motor neurons from SOD1^{G93A} astrocyte toxicity *in vitro*

Astrocytes are recognized to be key players in triggering MN death and disease progression in ALS.¹² Previous studies showed that astrocytes derived from SOD1^{G93A} mice are toxic to wild-type MNs in co-culture systems.^{28,34} To directly test whether our *in vivo* observations in the SOD1^{G93A} mice were linked to ADSC-mediated protection against toxic astrocytes, we took advantage of a separated triple-co-culture method in which ADSCs are physically separated from MN/astrocyte mixed co-cultures but able to communicate through the exchange of soluble factors (**Figure 5A**). Briefly, healthy wild-type murine Hb9-EGFP-MNs were co-cultured with mouse cortical astrocytes (mAstrocytes) derived from either NTg or SOD1^{G93A} genetically matched mice. mADSCs were seeded onto modified glass coverslips so to be added on top of the astrocyte/MN mixed co-culture without being physically in contact.²⁸ mAstrocytes were isolated and expanded from symptomatic (90 day old) SOD1^{G93A} mice and age-matched control NTg mice. By flow cytometry analysis, the astrocyte cultures were strongly positive for the astrocytic marker CD44 (>98% of cells) and largely depleted (<0.5% of cells) of cells positive for the microglial marker CD11b (**Figure S5**). Hb9-EGFP-MNs were obtained from mouse embryonic stem cells (mESCs) containing an EGFP gene under the MN-specific Hb9 promoter³⁵ and added to the astrocytes at day 7 of differentiation. At day 1 and day 7 of co-culture, Hb9-EGFP-MNs were imaged and counted. After 7 days in culture, there was a modest

but significant reduction (15%, $p = 0.008$, 2-way ANOVA with Tukey's test; **Figures 5B and 5C**) in survival of Hb9-EGFP-MNs in the SOD1^{G93A} astrocyte cultures compared with control NTg cultures, confirming that SOD1^{G93A} astrocytes are toxic and/or less able to support MN survival *in vitro*.^{28,36} The presence of ADSCs in the SOD1^{G93A} co-culture resulted in a significant increase of $\sim 23\%$ in MN viability compared with untreated SOD1^{G93A} cultures, abolishing the toxicity observed under basal conditions ($p = 0.0002$, 2-way ANOVA with Tukey's test; **Figures 5B and 5C**). Furthermore, MN survival in SOD1^{G93A} cultures containing ADSCs was $\sim 7\%$ higher than untreated NTg culture ($p = 0.043$, 2-way ANOVA with Tukey's test; **Figures 5B and 5C**). Interestingly, ADSCs also affected NTg astrocyte/MN co-cultures, improving MN survival by 15% ($p = 0.0021$, 2-way ANOVA with Tukey's test; **Figures 5B and 5C**). Given that in the presence of ADSCs an increase in MN survival was also observed in the control NTg astrocyte cultures, further co-culture experiments were carried out in order to determine whether the mechanism of protection was due to direct MN support rather than the ability of ADSCs to reduce the ALS astrocyte toxicity. Hb9-EGFP-MNs were seeded on laminin-coated plates and cultured for 3 days alone or in the presence of ADSCs (separated co-culture). The relative percentage of MN survival from day 1 to day 3 was then calculated and compared. Although non-statistically significant, an increase of $\sim 17\%$ in MN survival was observed when the motor neurons were co-cultured with ADSCs ($p = 0.3613$, paired t test; **Figure S6**).

ADSCs secrete VEGF and IGF-1 and modulate the secretion of these neurotrophic factors by mouse astrocytes

One of the proposed mechanisms of neuroprotection by ADSCs is their ability to secrete high levels of growth factors including vascular endothelial growth factor (VEGF) and insulin-like growth factor-1 (IGF-1).^{23,37} Moreover, there is evidence that these cells have the ability to respond differently according to the external stimuli to which they are exposed.^{38,39} Here, by using a separated co-culture method (**Figure 6A**), we evaluated the secretion of VEGF and IGF-1 by ELISA in supernatants of control unstimulated ADSCs and ADSCs co-cultured with either NTg or SOD1^{G93A} astrocytes. Separated co-cultures of ADSCs and astrocytes were maintained for 48 h. At the end of the 48-h co-culture ADSCs and astrocytes were separated and cultured alone for 24 h. The supernatant from both astrocytes and ADSCs was collected and growth factor release measured. In monocultures, ADSCs were able to secrete detectable levels of both

Figure 2. Survival and distribution of transplanted EGFP-ADSCs in SOD1^{G93A} mice

(A–D) Week 1 post-injection. (E–H) Week 2 post-injection. (I–L) Week 3 post-injection. (M–P) Week 4 post-injection. (Q–T) PBS injection. At 1 week from post-injection, clusters of EGFP-ADSCs were mostly found within the ventricular system close to the site of injection and in the IV ventricle (A), at the base of the brainstem (B), in the lateral recesses (C), and within the subarachnoid space of the spinal cord at cervical, thoracic, and lumbar levels (D). After 2 weeks, the majority of GFP⁺ cells were found in the IV ventricle (E) and in the lateral recesses close to the choroid plexus (G). Cells were also detected in the cisterna pontine and around the brainstem, where a few cells migrated into the parenchyma (F). EGFP-ADSCs in the subarachnoid space of the spinal cord migrated close to both dorsal and ventral roots; however, no cells were found to penetrate through the meninges (H). After 3 weeks, cells were still present in the IV ventricle (I) and in the cisterna pontine (J); however, the majority of the cells were detected in the lateral recesses (K). Cells were also detected in the subarachnoid space of the spinal cord close to ventral and dorsal roots especially at cervical and thoracic levels, with a few cells surviving in the lumbar enlargement (L). After 4 weeks from injection, the survival of ADSCs markedly decreased. A few cells were detected in the ventricular system and in the spinal cord meninges (M–P). No signal was detected in control PBS-injected mice (Q–T). Images were acquired with the IN Cell 2000 analyzer (GE Healthcare). Nuclei were stained with DAPI. Scale bars: 200 μm all. IV Ve, fourth ventricle; Bs, brainstem; Cb, cerebellum; CM, cisterna magna; Cp, cisterna pontine; Lr, lateral recess; ChP, choroid plexus; Cc, central canal; Dh, dorsal horn; Dr, dorsal root; Mg, meninges; ScLr, spinal cord lumbar region; Vr, ventral root.

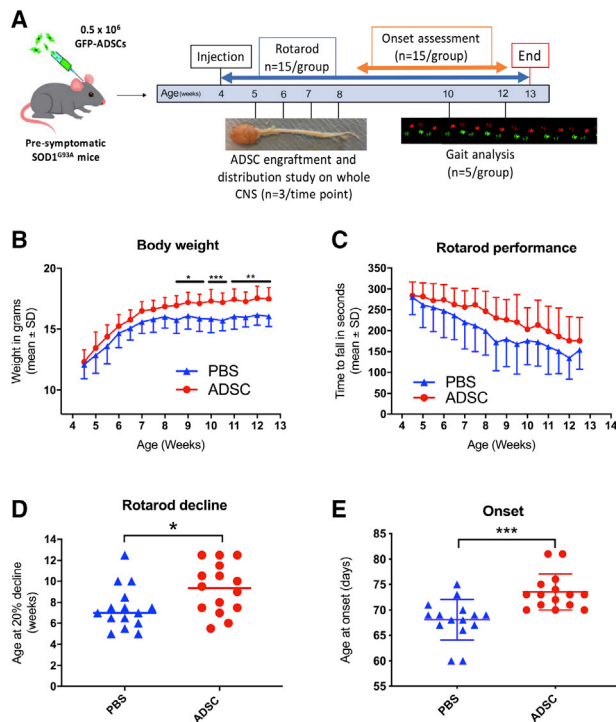


Figure 3. Intrathecal transplantation of ADSCs in SOD1^{G93A} mice delays motor function decline and onset of visible signs of disease

(A) Schematic diagram showing the "rapid" pre-clinical protocol in SOD1^{G93A} mice. Mice were injected with either 500,000 EGFP-ADSCs or PBS via the cisterna magna at 30 days of age (4 weeks) (n = 15 per group). Body weight and motor performance were monitored twice per week. Gait analysis was performed at day 70 and day 84 with the use of the CatWalk on a subset of the main cohort (n = 5 per group). During the study, EGFP-ADSC mice (n = 3 per group per time point) were sacrificed to evaluate engraftment and survival of EGFP-ADSCs. The study terminated at day 90 (week 13). (B) ADSC-injected mice gained significantly more weight compared with PBS-injected mice (p < 0.0001 for overall treatment effect, 2-way ANOVA; p values for Bonferroni's post tests at individual time points as indicated). (C) Treated mice showed overall improved motor performance on the rotarod task (p = 0.039, 2-way ANOVA). (D) Motor decline measured as the time taken to reach 20% reduction from peak of performance on the rotarod was significantly delayed (median 7 weeks for PBS injected, 9.5 weeks for ADSC injected, p = 0.0026, Mann-Whitney U test). (E) Onset of visible signs of disease defined as the presence of tremor and a hindlimb splay defect was significantly delayed in mice receiving ADSC treatment (68 ± 4 days for PBS, 73.5 ± 3.5 days for ADSC, p = 0.0005, unpaired t test). Error bars denote SD; n = 15 per group. *p < 0.05, **p < 0.01, ***p < 0.001, ****p < 0.0001.

VEGF and IGF-1 (Figures 6B and 6C). Notably, compared with monocultures, VEGF secretion in ADSCs was increased by ~27% after co-culture with NTg astrocytes (p = 0.0135, 1-way ANOVA with Tukey's test; Figure 6B) and by ~46% after co-culture with SOD1^{G93A} astrocytes (p = 0.0002, 1-way ANOVA with Tukey's test; Figure 6B). Interestingly, co-culture with SOD1^{G93A} astrocytes, but not with NTg astrocytes, induced ADSCs to secrete significantly higher levels of IGF-1 (p = 0.0003, 1-way ANOVA with Tukey's test; Figure 6C). ADSCs also seem to be able to modulate the expression levels of growth factors in astrocytes.^{22,40} Thus, we evaluated the secretion of

VEGF and IGF-1 in both NTg and SOD1^{G93A} astrocytes following separated co-culture with ADSCs (Figure 6A). At basal levels, SOD1^{G93A} astrocytes secreted a significantly higher amount of VEGF compared with NTg astrocytes (p = 0.0001, 1-way ANOVA with Tukey's test; Figure 6D). Interestingly, ADSC treatment increased the secretion of VEGF in NTg astrocytes (p = 0.0178, 1-way ANOVA with Tukey's test; Figure 6D), whereas it did not alter VEGF secretion in SOD1^{G93A} astrocytes. In contrast, secretion of IGF-1 from untreated SOD1^{G93A} astrocytes was significantly reduced compared with untreated control NTg astrocytes (p < 0.0001, 1-way ANOVA with Tukey's test; Figure 6E). The presence of ADSCs in the culture enhanced the secretion of IGF-1 in both NTg and SOD1^{G93A} astrocytes. In particular, IGF-1 secretion in SOD1^{G93A} astrocytes was increased by ~5-fold (p = 0.0386, 1-way ANOVA with Tukey's test; Figure 6E).

ADSCs reduce secretion of inflammatory mediators by SOD1^{G93A} mouse astrocytes

Among several mechanisms by which ALS astrocytes exert neural toxicity, increased secretion of inflammatory factors such as cytokines and chemokines has been demonstrated previously.^{12,41,42} Given their immunomodulatory properties, we investigated whether, through paracrine mechanisms, ADSCs could affect SOD1^{G93A} astrocytes by inhibiting the secretion of inflammatory mediators such as tumor necrosis factor (TNF)- α , interleukin (IL)-6, IL-1 β , and MCP-1. After the separated co-culture experiment (Figure 7A), the secretion of pro-inflammatory cytokines was measured in the supernatant of NTg and SOD1^{G93A} astrocytes with the use of the Multiplex Cytometric Bead Array (CBA) immunoassay. Under basal conditions (monocultures), levels of TNF- α were slightly increased in the SOD1^{G93A} astrocyte supernatant compared with the NTg astrocyte culture; however, the difference did not reach statistical significance (p = 0.2045, 1-way ANOVA with Sidak's test; Figure 7B). SOD1^{G93A} astrocytes secreted significantly higher levels of IL-6 (p < 0.0001, 1-way ANOVA with Sidak's test; Figure 7C) and MCP-1 (p < 0.0001, 1-way ANOVA with Sidak's test; Figure 7E) compared with NTg control astrocytes, whereas no difference was found in IL-1 β secretion (Figure 7D). Treatment with ADSCs inhibited the secretion of all four cytokines tested in SOD1^{G93A} astrocytes (Figures 7B–7E). In particular, after co-culture with ADSCs secretion of TNF- α was reduced by 69% (p = 0.0025, 1-way ANOVA with Sidak's test; Figure 7B), IL-6 by 68% (p < 0.0001, 1-way ANOVA with Sidak's test; Figure 7C), and MCP-1 by 22% (p < 0.0001, 1-way ANOVA with Sidak's test; Figure 7E), whereas IL-1 β levels were not detectable in supernatant from ADSC-treated astrocytes (Figure 7D).

ADSCs protect MNs from human ALS iAstrocyte toxicity *in vitro*

It has been shown that induced astrocytes (iAstrocytes) derived from ALS patients (with familial or sporadic disease) are toxic to MNs in culture.^{30,43} Here, we investigated whether the neuroprotective effect of ADSCs on Hb9-EGFP-MNs in mouse SOD1^{G93A} astrocyte co-cultures could be translated to a human model of disease. Importantly, this allowed us to test the therapeutic potential of ADSCs in both sporadic (sALS) and familial (fALS) cases of ALS (see Table S1 for patient

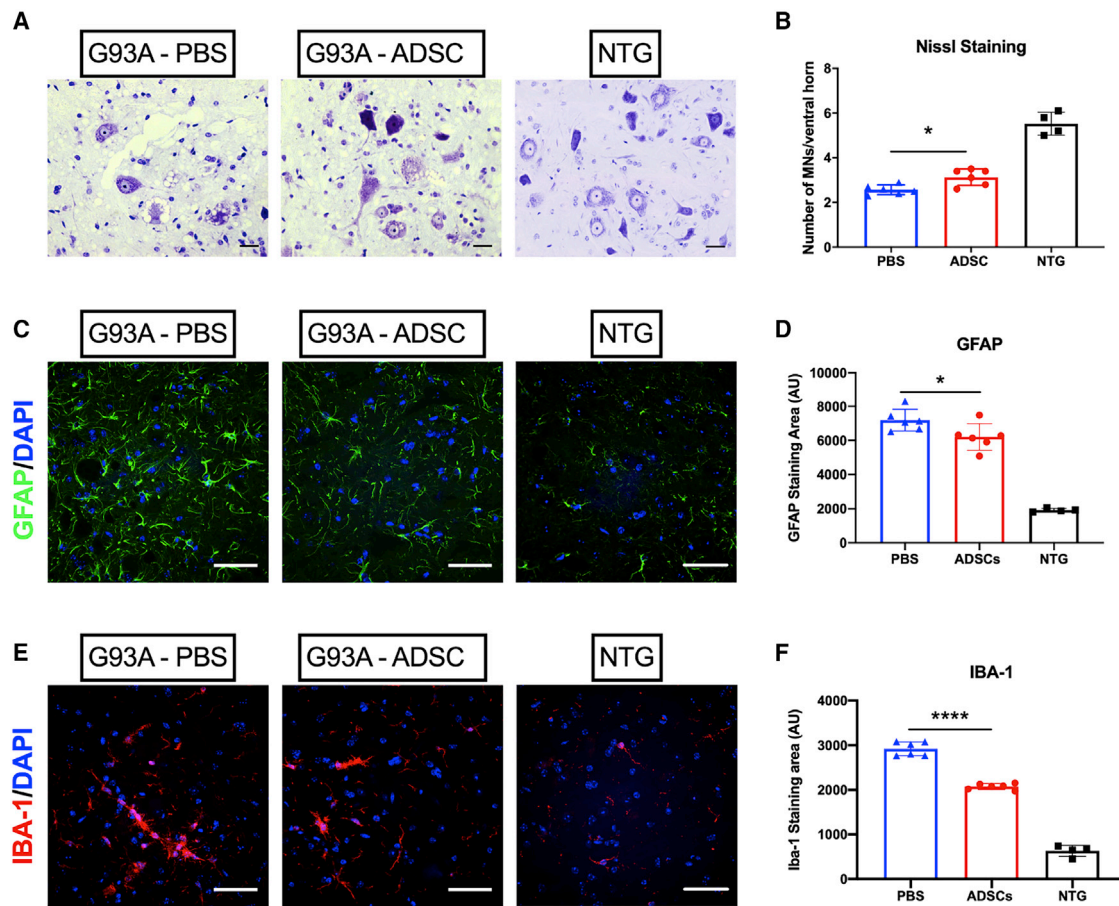


Figure 4. ADSCs protect MNs and reduce neuroinflammation in SOD1^{G93A} mice

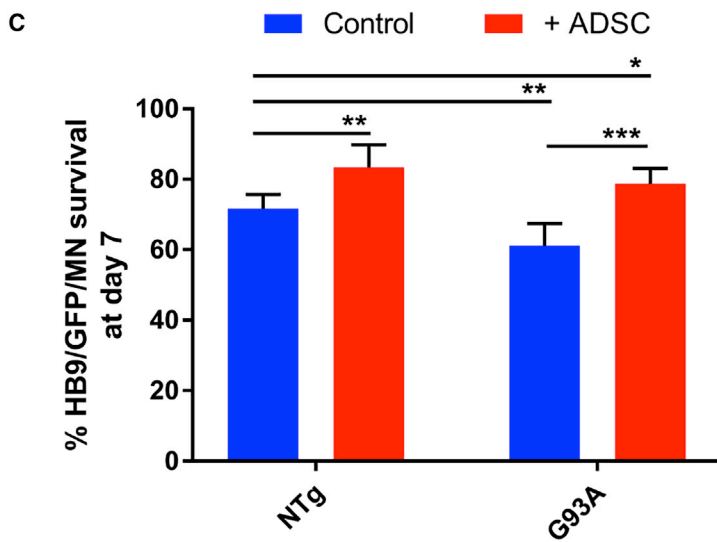
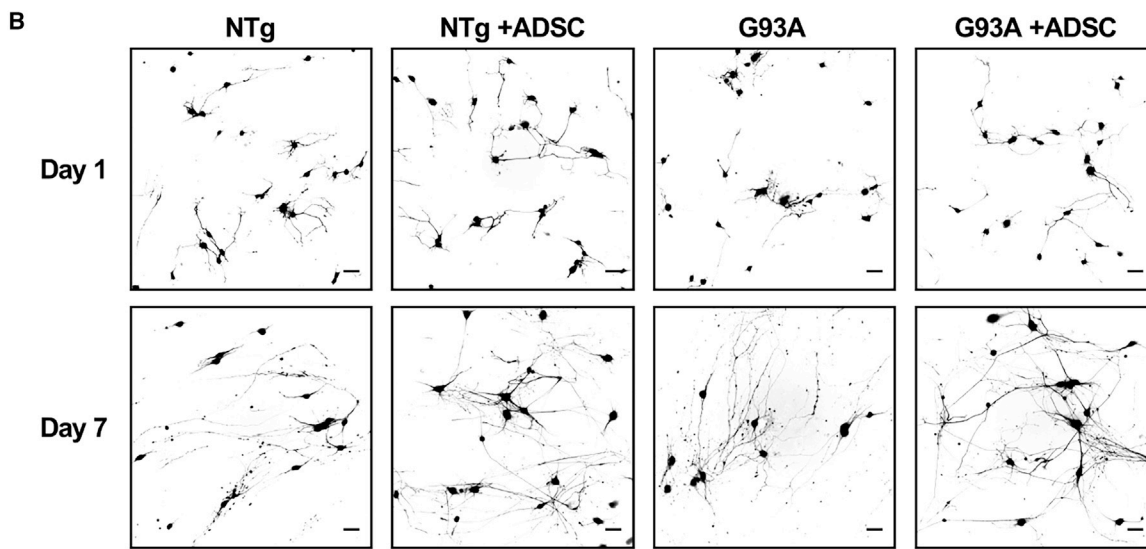
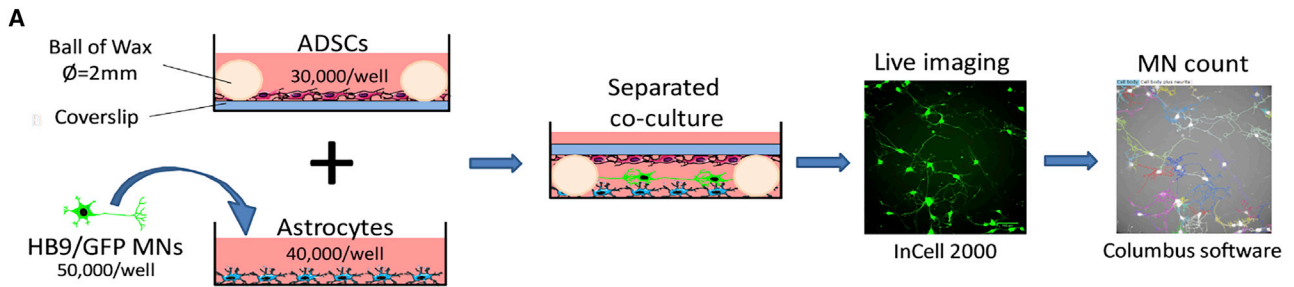
PBS-injected mice (n = 6), ADSC-injected mice (n = 6), and wild-type non-transgenic (NTG) mice (n = 4) at day 90 were sacrificed and lumbar spinal cords processed for histological examination. (A) Representative Nissl-stained lumbar spinal cord ventral horns. (B) The number of MNs was higher in ADSC-treated mice compared with the vehicle (2.6 ± 0.2 MNs/ventral horn in PBS versus 3.1 ± 0.4 MNs/ventral horn in ADSC, $p = 0.0434$, 1-way ANOVA with Tukey's multiple comparison test). (C) Representative images of GFAP staining in ventral horn of PBS-injected, ADSC-injected, and NTG mice. See also Figure S4A. (D) Quantification of GFAP staining measured as total staining area. Astrocyte activation was reduced in ADSC-transplanted mice ($7,191 \pm 635 \mu\text{m}^2$ in PBS versus $6,203 \pm 774 \mu\text{m}^2$ in ADSC, $p = 0.413$, 1-way ANOVA with Tukey's multiple comparison test). (E) Representative images of IBA-1 staining in PBS-injected, ADSC-injected, and NTG mice. See also Figure S4B. (F) IBA-1 total staining area quantification showing reduced microgliosis in ADSC-transplanted mice compared with the vehicle ($2,921 \pm 154 \mu\text{m}^2$ for PBS versus $2,075 \pm 67 \mu\text{m}^2$ for ADSC, $p < 0.0001$, 1-way ANOVA with Tukey's multiple comparison test). Data are presented as mean \pm SD. Scale bars: 50 μm all.

details), an approach not possible for sALS because of the lack of *in vivo* models. As expected, MN survival in ALS-derived iAstrocyte cultures was reduced compared with control-derived iAstrocytes (Figure 8). Remarkably, the presence of mADSCs protected MNs from both sALS and fALS iAstrocytes regardless of the genetic subtype. Interestingly, the protective effect was observed for some but not all patients tested, with one sporadic and one SOD1-linked iAstrocyte line being less responsive to the benefits of ADSC exposure.

DISCUSSION

Previous studies demonstrated the efficacy of intrathecal transplantation of MSCs into SOD1^{G93A} rodents (reviewed in Ciervo et al.¹⁴). Moreover, phase I and II clinical trials have demonstrated that the in-

jection of MSCs directly into the CSF of ALS patients is safe and well tolerated.^{44–46} However, further pre-clinical investigation to shed light on the mechanisms of protection mediated via effects on neurons and/or non-neuronal cells and the identification of the best source of MSCs is still needed. Most of the previous studies transplanted MSCs derived from the bone marrow or umbilical cord. However, adipose tissue may provide a better adult stem cell source because of the ease and efficiency of obtaining clinically relevant numbers of MSCs. In the current study, we evaluated the therapeutic potential of mADSCs in ALS by using both *in vivo* and *in vitro* models of disease. Studies evaluating the therapeutic potential of MSCs in the SOD1^{G93A} murine model of ALS have been mostly carried out by transplanting human cells.¹⁴ However, immunosuppression in recipient rodents was often required in order to avoid rejection of the



(legend on next page)

transplanted human stem cells. The use of immunocompromised ALS animals for the study of MSC transplantation is disadvantageous for several reasons. Given that one of the protective mechanisms of action of MSCs in ALS is based upon their immunomodulatory activity, the use of immunosuppressive agents could significantly alter and/or mask important features of the transplanted cells and how they respond to the ALS microenvironment. Moreover, an important characteristic of MSCs is their low immunogenic profile, which would facilitate both autologous and allogeneic transplantation in humans. So the introduction of an immunosuppressive regime when investigating the therapeutic potential of MSCs *in vivo* could be controversial. For these reasons, the *in vivo* work here presented focused on the use of mADSCs, which avoided the need for immunosuppressive agents.

Our results indicate that a single intrathecal dose of ADSCs injected into SOD1^{G93A} mice at the pre-symptomatic stage is able to significantly improve motor performance and delay disease onset through MN protection and attenuation of glial activation. These data provide evidence that ADSCs possess therapeutic properties similar to those of BM-MSCs and umbilical cord MSCs (UC-MSCs) when injected into the CSF of ALS mice. Importantly, in contrast to other studies using transgenic SOD1^{G93A} mice on the mixed B6SJL/F1/J genetic background, here mice of defined C57BL/6J genetic background were used. The use of the mixed SLJB6 genetic background can lead to a high degree of biological variability, which confounds interpretation of the data.^{33,47} In contrast, our model shows minimal genetic variation, reduced background noise in biological readouts, and robust reproducibility of disease.³³ A limitation of the present work is that cells were transplanted before clinical signs of the disease and mice were not followed until the end-stage. However, deficits in motor performance in our model can be detected before clinical signs of disease become evident.⁴ This initial deficit can be measured as a 20% reduction in rotarod performance, which correlates with early denervation of motor endplates.³³ This is an important feature of the model, enabling investigation of therapeutic strategies during early stages of disease, which may be crucial in the development of therapies for human ALS.⁴⁸ Of interest, in human patients decline in physical performance and features of neurodegeneration are observed before the diagnosis of ALS is established.^{49,50} Therefore, here we demonstrated that ADSCs protected MNs during the first stages of neuronal degeneration characterized by the initial loss of neuromuscular junctions (NMJs).

We also qualitatively evaluated the distribution and engraftment of EGFP-ADSCs throughout the CNS over time, showing that ADSCs are able to survive in ALS mice for up to 1-month post-transplantation. Injection through the cisterna magna allowed the cells to widely distribute within the brain ventricular system and to reach the level of the lumbar spinal cord. In agreement with other studies,^{18,20,51} ADSCs did not migrate into the spinal cord parenchyma, thus reinforcing the notion that the beneficial effects observed are due to the paracrine activity of ADSCs, with potential medium-term effects, since increased numbers of surviving MNs and reduced glial activation were observed ~2 months after stem cell application. Although intrathecal delivery may represent the preferred route of administration of MSCs in ALS patients, methods to improve cell migration and engraftment into the spinal cord parenchyma are needed. If on the one hand clinical benefits could be achieved without integration into the host spinal cord parenchyma, on the other hand multiple and repeated injections might be necessary to achieve prolonged benefits. This may represent an important limitation, because of the large amount of cells needed and consequently the high costs related to manufacturing, cell banking, and patient care/hospitalization. To better understand whether intrathecal stem cell injection could effectively produce beneficial effects in patients further studies are needed. In our study ADSCs were injected at a pre-symptomatic stage, during which inflammatory chemical signals such as chemokines and cytokines necessary to activate or induce the homing properties of ADSCs might not yet have been secreted at biologically relevant concentrations.⁵² At a later stage of disease, a sustained inflammatory milieu may allow MSCs to enter the parenchyma.¹⁷ Future studies injecting cells after the onset of clinical signs of disease to evaluate engraftment, disease progression, and survival are needed. In particular, it would be highly informative to determine whether multiple repeated injections of ADSCs would be more effective compared with a single administration.

Previous studies showed that conditioned medium from MSCs protected MNs against mechanical, oxidative, and apoptotic stress *in vitro*.^{23,40,53} However, in these studies application of external stimuli such as treatment with H₂O₂, staurosporine, or manual scratch were necessary in order to induce MN damage. In our study, through paracrine mechanisms, ADSCs were able to protect MNs from intrinsic SOD1^{G93A} astrocyte toxicity. Thus, for the first time the neuroprotective potential of ADSCs in ALS models is demonstrated by

Figure 5. ADSCs protect MNs from SOD1^{G93A} astrocyte toxicity and promote MN survival in NTg astrocyte cultures

(A) Schematic diagram showing astrocyte/Hb9-EGFP-MN/ADSC separated triple-co-culture system. MNs are seeded on a confluent layer of astrocytes and ADSCs onto glass coverslips. Culture plates are imaged at days 1 and 7 with the IN Cell 2000 analyzer to identify live GFP-MNs. MN quantification is performed with the use of Columbus software, which allows selection and counting of only GFP-positive cell bodies with at least two processes. (B) Representative images of Hb9-EGFP-MNs at days 1 and 7 of co-culture with SOD1^{G93A} or NTg astrocytes under basal conditions and in the presence of ADSCs (scale bars: 50 μ m). (C) Quantification of motor neuron survival after 7 days of co-culture. SOD1^{G93A} astrocytes are toxic to MNs compared with NTg astrocyte co-cultures (71% \pm 4% MN survival in NTg versus 61% \pm 6% in G93A). ADSCs protected MNs from G93A astrocyte toxicity (61% \pm 6% in untreated versus 79% \pm 4% in ADSC treated) and increased MN survival compared with untreated NTg astrocytes (7%). ADSCs increased MN survival on NTg astrocyte co-cultures compared with untreated NTg astrocytes (71% \pm 4% MN survival in untreated versus 83% \pm 6% in ADSC treated). MN quantification represents 3 independent experiments, where each experiment is in triplicate and consists of a different astrocyte preparation (2-way ANOVA, plus Tukey's multiple comparison test). **p* < 0.05, ***p* < 0.01, ****p* < 0.001. Error bars represent SD. G93A, SOD1^{G93A} astrocytes; MN, motor neurons; NTg, non-transgenic astrocytes.

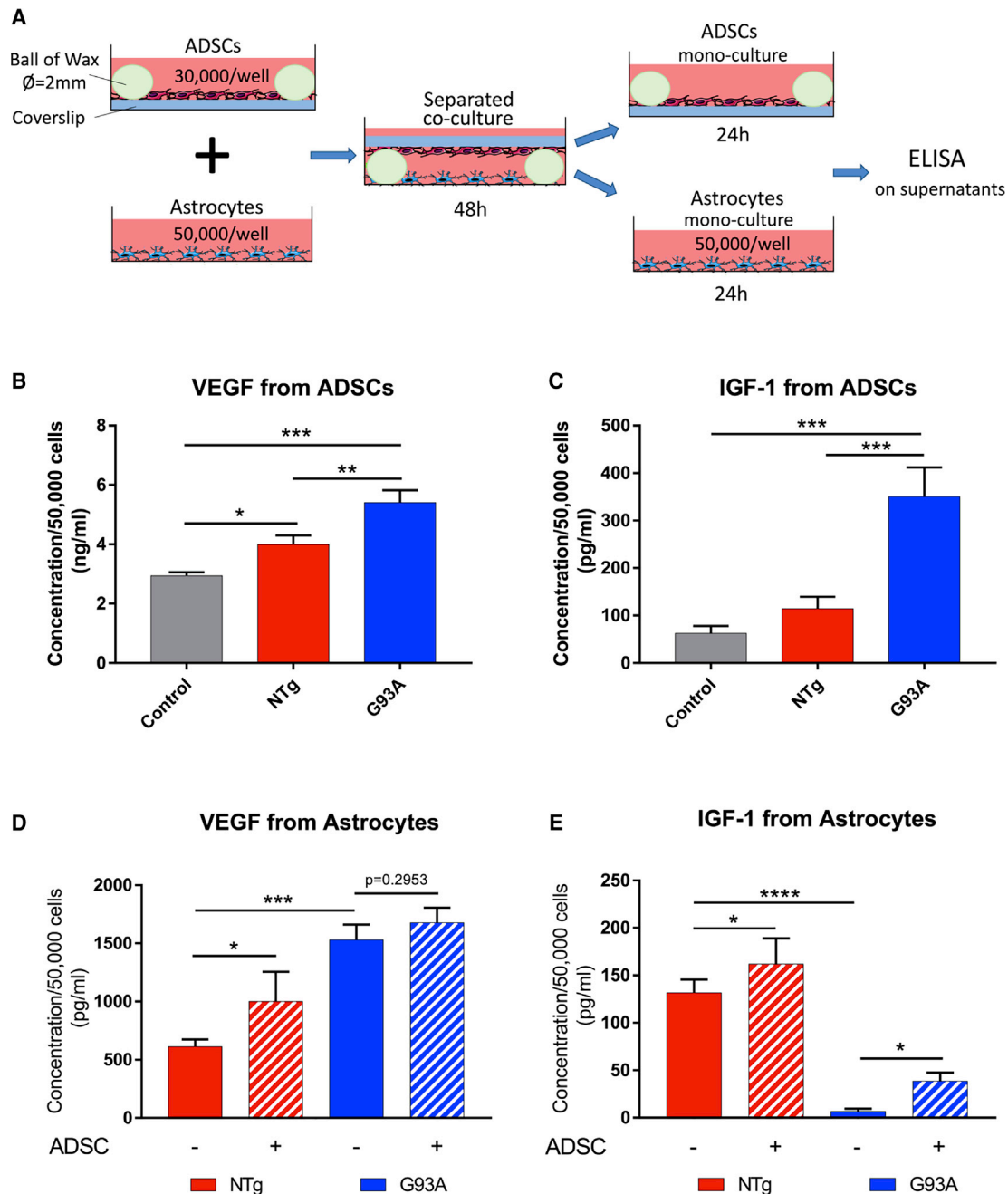


Figure 6. Modulation of VEGF and IGF-1 secretion in ADSC/mAstrocyte separated co-cultures

(A) Schematic diagram showing the astrocyte/ADSC separated co-culture system. Astrocytes are seeded on plastic culture wells and ADSCs onto glass coverslips. After 48 h of separated co-culture, coverslips containing ADSCs are removed from the astrocytes and both ADSCs and astrocytes are maintained as monocultures for a further 24 h. Supernatant from astrocytes and ADSCs is collected and the amount of growth factors measured by ELISA. (B) Without any stimulus, ADSCs secreted 2.94 ± 0.1 ng/mL of VEGF. The presence of either NTg or SOD1^{G93A} astrocytes induced ADSCs to secrete significantly more VEGF compared with ADSC monocultures. Co-culture with SOD1^{G93A} astrocytes induced significantly higher secretion of VEGF compared with ADSCs co-cultured with NTg astrocytes (3.99 ± 0.3 ng/mL in NTg versus 5.4 ± 0.4 ng/mL in SOD1^{G93A}). (C) Secretion levels of IGF-1 were significantly increased in ADSCs co-cultured with SOD1^{G93A} astrocytes compared with control ADSC monocultures (62.39 ± 15.11 pg/mL in monocultures versus 350.2 ± 61.79 pg/mL in SOD1^{G93A}) and compared with ADSCs cultured with NTg astrocytes (114.5 ± 24.8 pg/mL in NTg versus 350.2 ± 61.79 pg/mL in SOD1^{G93A}). (D) At basal levels SOD1^{G93A} astrocytes secreted significantly more VEGF than control NTg astrocytes (612 ± 62.5 pg/mL for NTg versus $1,531 \pm 129.1$ pg/mL for SOD1^{G93A}). Co-culture with ADSCs induced a significant increase in VEGF secretion in NTg astrocytes

(legend continued on next page)

adopting a less artificial *in vitro* system that more closely recapitulates the environment in human ALS.

In agreement with recent evidence that astrocytes actively participate in inflammation-mediated neuronal damage,^{12,41} SOD1^{G93A} astrocytes secreted enhanced levels of pro-inflammatory cytokines compared with NTg astrocytes. Notably, ADSCs modulated astrocytic functions by reducing the secretion of pro-inflammatory mediators such as IL-6, MCP-1, IL-1, and TNF and by enhancing the production of the anti-inflammatory and neuroprotective factor IGF-1. Thus, in addition to immunomodulation of peripheral immune cells and resident microglia, MSCs showed the capacity to reduce the pro-inflammatory signature in adult SOD1^{G93A} astrocytes, which actively contribute to neuroinflammation.^{40,54–56} ADSCs secreted biologically relevant amounts of VEGF and IGF-1, which were further increased after co-culture with SOD1^{G93A} astrocytes, confirming the capacity of MSCs to respond to the toxic ALS environment by producing factors that can directly and indirectly support MNs.^{57–59} For instance, in independent studies IGF-1 has been shown to not only protect MNs from excitotoxicity but also inhibit the inflammatory response in lipopolysaccharide (LPS)-stimulated astrocytes *in vitro* and to reduce astrogliosis in a rat model of brain injury.^{60–62} VEGF has well-described neuroprotective actions and has been shown to protect MNs against glutamate excitotoxicity, as well as stimulating axonal growth and promoting synaptic plasticity.^{57,63} Moreover, through the release of VEGF, IGF-1, and hepatocyte growth factor (HGF), ADSCs improved the glutamate recycling function in SOD1^{G93A} astrocytes and protected neuronal cells from apoptosis induced by oxidative stress.^{23,58,64}

It is worth mentioning that a large body of research has explored the therapeutic potential of directly delivering VEGF or IGF-1 into ALS animal models.⁶⁵ Interestingly, several strategies to enhance the concentration of these factors, alone or in combination, in brain, spinal cord, or muscle of SOD1^{G93A} mice improved motor performance, slowed down disease progression, and extended lifespan through MN protection, preservation of NMJ, and reduction of microgliosis. Unfortunately, several clinical trials assessing the safety and efficacy of direct injection of growth factors in ALS patients have fallen short of expectations. Several hypotheses were raised to explain these failures, such as route of administration, dose, the inability of the factors to cross the blood-brain barrier (BBB), and possibly the need to use a combination of different growth factors that operate synergistically to achieve therapeutic benefits.⁶⁶ Although we do not have direct evidence showing that IGF-1 and VEGF released by ADSCs are responsible for the reduced MN death observed in our triple co-culture system, the secretion of these factors from ADSCs is likely to have

contributed significantly to the therapeutic effects observed in our studies. Further studies using neutralizing antibodies against VEGF and IGF-1, or the use of RNA interference, may help to further elucidate the molecular mechanisms of protection.

Together with previous reports, we have presented evidence that the therapeutic potential of ADSCs arises from a combination of mechanisms that not only directly support MNs through, for example, the uninterrupted secretion of growth factors and cytokines but also by modulating astrocyte and microglial functions, culminating in the generation of a neuroprotective environment.^{22,54,55} In addition to growth factors and cytokines, ADSCs secrete exosomes, which protected MN-like NSC-34 SOD1^{G93A} cells from an oxidative insult and also alleviated protein aggregation and mitochondrial dysfunction in differentiated SOD1^{G93A} neuronal stem cells.^{67,68}

Although SOD1^{G93A} mice represent a robust and well-characterized model of ALS, SOD1 mutations are responsible for a small percentage of human ALS cases and several promising therapeutic approaches tested in this model have failed to translate into human benefit.⁴⁷ Here, as a proof of concept for translation into the human disease, we showed that ADSCs have the capacity to protect MNs from iAstrocyte toxicity, using cells derived from human patients with either sporadic or familial disease caused by mutations in the *C9orf72* or *SOD1* genes. Interestingly, each iAstrocyte cell line responded to the ADSC treatment to a different degree, with two cell lines that did not show a significant positive response. This finding highlights the importance of controlling for patient heterogeneity in clinical trial enrollment and the need for patient stratification methods when evaluating therapies in ALS. Further studies adopting our *in vitro* system and investigations aimed to unravel the molecular mechanisms of action of ADSCs on human iAstrocytes are of great interest, potentially enabling the identification of responders and, more importantly, of potential ADSC biological markers predictive of a positive/negative therapeutic response.

MATERIALS AND METHODS

Isolation and expansion of mouse adipose-derived stem cells

mADSCs were isolated from 8- to 10-week-old female C57BL/6J mice as previously described with minor modifications.⁶⁹ Mice were sacrificed by cervical dislocation, and inguinal (subcutaneous) fat pads were aseptically removed and collected into a 50-mL Falcon tube containing sterile ice-cold Hank's balanced salt solution with Ca²⁺ and Mg²⁺ (HBSS) (Gibco, Waltham, MA, USA) and 50 U/mL penicillin-streptomycin (Pen/Strep) (Lonza, Basel, Switzerland). Before proceeding to the mechanical disruption of the tissue, lymph nodes were carefully removed to avoid leukocyte contamination. The tissue

(612 ± 62.5 pg/mL in untreated versus 1,001 ± 255.6 pg/mL in ADSC treated) but not in SOD1^{G93A} astrocytes. (E) Secretion levels of IGF-1 were significantly reduced in SOD1^{G93A} astrocytes compared with control NTg astrocytes (131.6 ± 13.92 pg/mL for NTg versus 6.6 ± 3 pg/mL for SOD1^{G93A}). The presence of ADSCs in the culture induced the secretion of IGF-1 in both NTg (131.6 ± 13.92 pg/mL in untreated versus 162 ± 27 pg/mL in ADSC treated) and SOD1^{G93A} (6.6 ± 3 pg/mL in untreated versus 38.6 ± 9 pg/mL in ADSC treated) astrocytes. Data are presented as mean ± SD; n = 3 separate experiments where each n consists of a different astrocyte preparation. Data analyzed with 1-way ANOVA plus Tukey's multiple comparison test. *p < 0.05, **p < 0.01, ***p < 0.001, ****p < 0.0001. G93A, SOD1^{G93A} astrocytes; NTg, non-transgenic astrocytes.

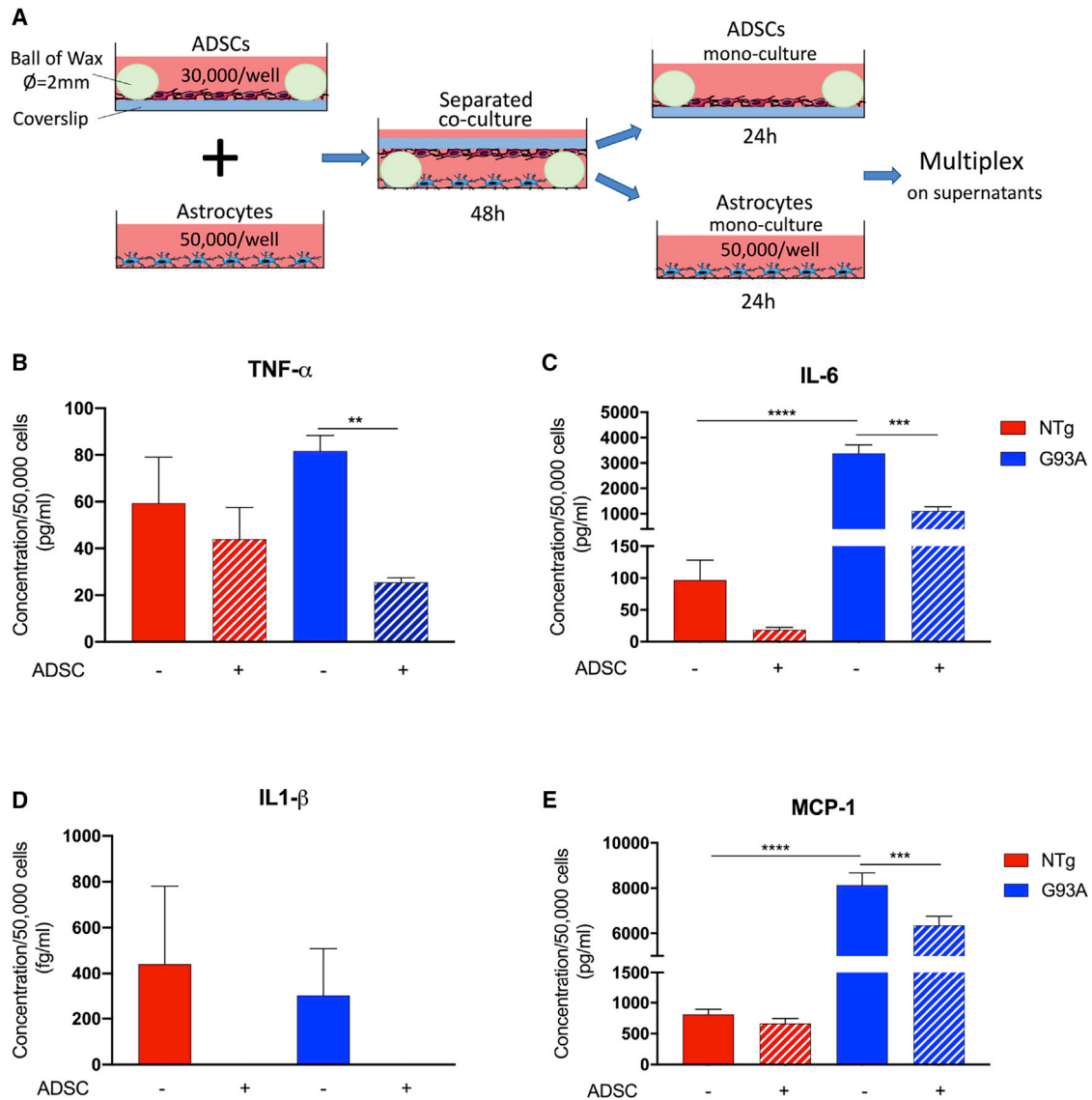


Figure 7. Increased secretion of inflammatory cytokines in $SOD1^{G93A}$ astrocytes is downregulated after co-culture with ADSCs

(A) $SOD1^{G93A}$ and control NTg astrocytes were seeded and grown as monocultures before addition of ADSCs previously seeded onto glass coverslips. For controls, empty coverslips were added to the astrocytes. Separated co-cultures were maintained for 48 h in basal astrocytic medium. Coverslips containing ADSCs were then removed and astrocytes cultured for 24 h before supernatant collection and measurement of cytokines/chemokines with the use of the Multiplex Cytometric Bead Array (CBA) immunoassay. (B) $SOD1^{G93A}$ astrocytes secreted more TNF- α compared with controls (59.4 ± 19.6 pg/mL for NTg versus 81.7 ± 6.7 pg/mL for $SOD1^{G93A}$), which decreased after ADSC exposure (25.45 ± 2 pg/mL). (C) $SOD1^{G93A}$ astrocytes secreted more IL-6 than control astrocytes (96.8 ± 31.4 pg/mL for NTg versus $3,374 \pm 339.2$ pg/mL for $SOD1^{G93A}$), which was reduced after co-culture with ADSCs ($1,104 \pm 167$ pg/mL). (D) No difference was found between $SOD1^{G93A}$ and control astrocytes in IL-1 β secretion (440 ± 340 fg/mL for NTg versus 301 ± 206 fg/mL for $SOD1^{G93A}$). However, no detectable levels of IL-1 β were found in the supernatant of ADSC-treated cultures. (E) Secretion levels of the chemokine MCP-1 were upregulated in $SOD1^{G93A}$ astrocytes (811 ± 83 pg/mL for NTg versus $8,133 \pm 543$ pg/mL for $SOD1^{G93A}$). ADSC exposure reduced secretion of MCP-1 ($6,346 \pm 414$ pg/mL). Data are presented as mean \pm SD; $n = 3$ separate experiments where each n consists of a different astrocyte preparation. Data analyzed with 1-way ANOVA plus Sidak's multiple comparison test. ** $p < 0.01$, *** $p < 0.001$, **** $p < 0.0001$. Error bars represent SD. G93A, $SOD1^{G93A}$ astrocytes; NTg, non-transgenic astrocytes.

was digested with 0.075% collagenase I (Sigma, St. Louis, MO, USA) and 2% bovine serum albumin (BSA) (Sigma, St. Louis, MO, USA) at 37°C in a water bath for 60–80 min with gentle shaking every 10 min. The resulting homogenate was then filtered through a 70- μ m sterile

mesh cell strainer (Fisher Scientific, Hampton, NH, USA) and centrifuged at $500 \times g$ for 5 min to obtain the stromal vascular fraction (SVF). Contaminating red blood cells were lysed with red blood cell lysis buffer (160 mM NaH_2Cl , 14 mM $NaHCO_3$, 0.1 mM EDTA;

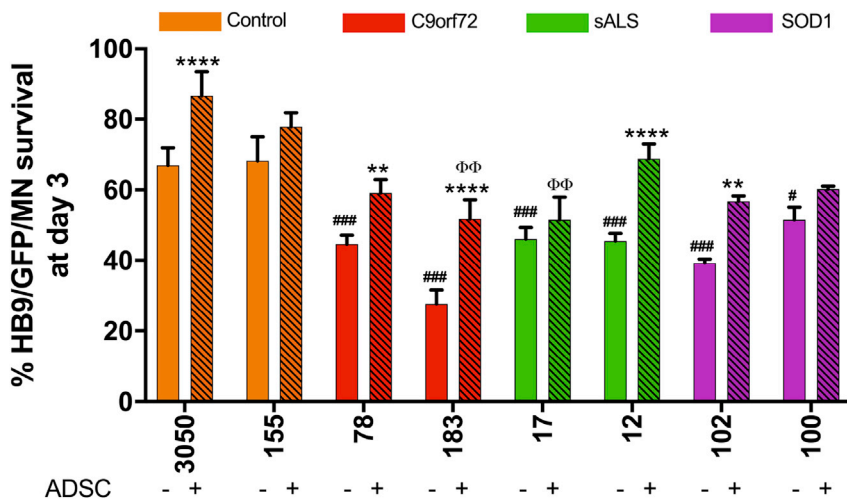


Figure 8. Effect of ADSCs on survival of murine Hb9-EGFP-MNs after co-culture with control and ALS-derived human iAstrocytes

The graph shows the percentage of MNs that survived from day 1 to day 3 of co-culture with human iAstrocytes in the presence or absence of mADSCs. The orange bars represent astrocytes derived from control patients; red bars astrocytes carrying the C9orf72 repeat expansion; green bars astrocytes derived from sporadic ALS patients; and purple bars astrocytes derived from patients with the SOD1^{A4V} mutation. MN survival was significantly reduced in iAstrocytes derived from ALS patients compared with control iAstrocytes obtained from healthy control donors. The presence of ADSCs protected MNs from iAstrocyte ALS neurotoxicity, restoring MN survival at levels sometimes comparable to those observed in control non-ALS cultures. The ability of ADSCs to reduce MN death appeared to be patient specific, since in the sALS Pat17 and SOD1 Pat100 iAstrocyte cultures ADSCs did not significantly improve MN survival, although a trend toward improved survival was

observed in both of these cases. Quantification is representative of 3 or 4 independent experiments, where each experiment is in quintuplicate. Data analyzed with 2-way ANOVA, plus Tukey's multiple comparison test, * $p < 0.05$, ** $p < 0.01$, *** $p < 0.001$, **** $p < 0.0001$; ## $p < 0.005$, ### $p < 0.0001$. Error bars represent SD. Asterisks denote significant differences between ADSC-treated and non-treated iAstrocytes; number signs denote significant differences between ALS-iAstrocytes and control iAstrocytes; phi symbols denote significant differences between ADSC-treated ALS-iAstrocytes and non-treated control iAstrocytes.

pH 7.3) for 7 min at room temperature (RT) in the dark. Cells were then filtered, washed in HBSS, and cultured in Dulbecco's modified Eagle's medium (DMEM) (Lonza, Basel, Switzerland) containing 4,500 mg/L glucose, L-glutamine, 10% fetal bovine serum (FBS) (MSC-Qualified, 13662-011, Gibco, Waltham, MA, USA), and 1% Pen/Strep. After 48 h, the non-attached cells and cellular debris were removed by washing in PBS and fresh complete medium was added. When cultures were 80% confluent, cells were detached with trypsin-Versene-trypsin-EDTA (Lonza, Basel, Switzerland) and plated for expansion at a seeding density of 5,000 cells/cm². For experiments, ADSCs were used at passages 3–5.

Flow cytometry

Cells were collected by trypsinization and counted, and viability was determined by the trypan blue (Sigma, St. Louis, MO, USA) exclusion method. Cells were not analyzed if viability was <90%. Cells were re-suspended in ice-cold flow cytometry (FC) buffer, consisting of PBS containing 2% FBS (Gibco, Waltham, MA, USA) and aliquoted into microcentrifuge tubes at a concentration of 5×10^5 cells/tube. After 10-min incubation on ice, cells were washed by centrifugation and incubated on ice for 30 min with the specific fluorescent labeled monoclonal antibody. The following antibodies were used: mouse anti-CD90-phycoerythrin (PE) ($0.15 \mu\text{g}/5 \times 10^5$ cells), mouse anti-CD44-allophycocyanin (APC) ($0.13 \mu\text{g}/5 \times 10^5$ cells), mouse anti-CD106-phycoerythrin-cyanine7 (PE-Cy7) ($0.20 \mu\text{g}/5 \times 10^5$ cells), mouse anti-CD45-fluorescein isothiocyanate (FITC) ($0.15 \mu\text{g}/5 \times 10^5$ cells), mouse anti-CD34-PE ($0.13 \mu\text{g}/5 \times 10^5$ cells), mouse anti-CD31-APC ($0.15 \mu\text{g}/5 \times 10^5$ cells), mouse anti-CD29-PE-Cy7 ($0.50 \mu\text{g}/5 \times 10^5$ cells), mouse anti-CD105-PE-Cy7 ($0.50 \mu\text{g}/5 \times 10^5$ cells), and mouse anti-CD11b-FITC ($0.13 \mu\text{g}/5 \times 10^5$ cells). Cells were also stained with an equal concentration of matched fluorescent

labeled isotype control antibodies. All the antibodies were purchased from BioLegend (San Diego, CA, USA). After the incubation period, cells were washed three times with FC buffer by centrifugation and transferred to 5-mL fluorescence-activated cell sorting (FACS) tubes (12×75 mm) (BD Biosciences, Franklin Lakes, NJ, USA).

Stained cells were acquired on a BD LSRII FACS instrument (BD Biosciences, Franklin Lakes, NJ, USA) and analyzed with FlowJo 7.6.1 (FlowJo LLC, Ashland, OR, USA). From each sample at least 10,000 single-cell events were collected.

Tri-lineage differentiation of ADSCs

By following the international guidelines released by the International Society for Cellular Therapy (ISCT) and by the International Federation for Adipose Therapeutics and Science (IFATS),³¹ the multilineage potential differentiation of ADSCs was assessed by adipogenic, osteogenic, and chondrogenic induction as described in the literature.^{25,70} All reagents for differentiation were purchased from Sigma-Aldrich (St. Louis, MO, USA) unless otherwise stated. For adipogenesis, passage 3 ADSCs growing on glass coverslips were incubated for 3 days in adipogenic induction medium (AIM) consisting of DMEM (Lonza, Basel, Switzerland) supplemented with 10% FBS (Gibco, Waltham, MA, USA), 1% Pen/Strep, 1 μM dexamethasone, 1 μM insulin, 200 μM indomethacin, and 0.5 mM 3-isobutyl-1-methylxanthine (IBMX). On the fourth day the AIM was switched to adipogenic maintenance medium consisting of DMEM plus 10% FBS, 1% Pen/Strep, 1 μM dexamethasone, 1 μM insulin, and 200 μM indomethacin. The medium was replaced every 3 days with fresh medium. To assess for spontaneous differentiation, ADSCs were cultured with complete control medium (DMEM, 10% FBS, and 10% Pen/Strep). Adipogenic differentiation was assessed after 2 weeks of induction

by oil red O (O-R-O) staining.⁷¹ Briefly, cells were washed with PBS and fixed with 4% paraformaldehyde (PFA) pH 7.4 at RT for 20 min. Next, the wells were washed twice with dH₂O for 5 min in agitation and stained with O-R-O working solution for 15 min at RT. After incubation, cells were washed three times with dH₂O for 5 min in agitation and rinsed once in 60% isopropanol in order to remove any excess of stain. Nuclei were counterstained with Mayer's hematoxylin, and coverslips were mounted with aqueous VectaMount mounting solution (VectaLabs, Burlingame, CA, USA). Images were then captured with an upright Nikon Eclipse Ni microscope (Nikon, New York City, NY, USA).

Osteogenesis was induced in confluent ADSC cultures with a differentiation medium consisting of DMEM supplemented with 10% FBS, 1% Pen/Strep, 0.1 μM dexamethasone, 50 μg/mL ascorbic acid, and 10 mM β-glycerolphosphate. Every 3 days, cells were fed with fresh osteogenic differentiation medium for a total of 2 weeks. For controls, ADSCs were cultured in complete control medium.

Osteogenic differentiation was confirmed by alizarin red staining.⁷² Cells were gently washed once with PBS and fixed for 30 min at RT with a fixation solution consisting of 39.7% dH₂O, 59.5% acetone, and 0.8% citrate concentrated solution (sodium citrate tribasic dehydrate 1 M). After fixation, cells were washed with PBS and stained with 2% alizarin red S for 45 min at RT. After the incubation period, cells were washed at least 5 times with dH₂O to remove any trace of free dye and rinsed in PBS. Coverslips were mounted on glass slides and visualized with the Nikon Eclipse Ni microscope (Nikon, New York, NY, USA).

Chondrogenic differentiation was performed on three-dimensional cell pellets.⁷⁰ ADSCs were detached with trypsin and centrifuged at 300 × g at RT for 4 min. Cells were then counted, and 0.5 × 10⁶ cells were aliquoted in 15-mL Falcon tubes. After a further centrifugation step, the supernatant was removed and pellets re-suspended with 500 μL of chondrogenic differentiation medium consisting of DMEM containing 1% FBS, 1% Pen/Strep, 1% insulin-transferrin-selenium (ITS) (Gibco, Waltham, MA, USA), 1% sodium pyruvate, 50 μg/mL ascorbic acid, 0.1 μM dexamethasone, and 10 ng/mL transforming growth factor β1 (PeproTech, Rocky Hill, NJ, USA). Cells were then centrifuged at 300 × g for 3 min at RT, and tubes were placed in an incubator without disturbing the pellet. Freshly prepared chondrogenic medium was changed every day for the first 3 days. From the fourth day onward, medium was changed every 3 days. For non-induced controls, pellets were cultured in the presence of control medium consisting of DMEM, 1% FBS, and 1% Pen/Strep.

Chondrogenesis was assessed after 3 weeks of differentiation by Alcian blue staining.⁷³ Cell pellets were washed twice in PBS and fixed in PFA 4% at room temperature for 30 min. Pellets were then washed in PBS and cryo-protected in 30% sucrose (w/v) in PBS at 4°C overnight (O/N). The day after, pellets were embedded in optimal cutting temperature compound (OCT) (CellPath, Newtown, UK) and rapidly

frozen on dry ice soaked in methanol. Frozen pellets were cut in 20-μm-thickness sections and collected on glass slides. For Alcian blue staining, tissue sections were acidified for 5 min at RT with 0.1 M HCl. Slides were then stained with Alcian blue 1% in 0.1 M HCl 1 h at RT. After incubation, sections were rinsed in 0.1 M HCl, washed with ddH₂O, and mounted.

Production and titration of EGFP-expressing lentiviral particles

The pLV-SIN-EGFP vector was a gift from Dr. Evangelia Karyka (University of Sheffield, Sheffield, UK). The pLV-EGFP plasmid is a HIV-1-based expression vector in which the transcription of EGFP is driven by the mouse phosphoglycerate kinase (mPGK) promoter. The vector contains all the viral processing elements for the production of self-inactivating (SIN) third-generation lentiviral particles.

Lentivirus was produced from co-transfection of HEK293T cells with the transfer plasmid pLV-SIN-EGFP and the three packaging plasmids pCMVΔ8.92, pRSV-Rev, and pMDG2.

One day before transfection, HEK293T cells were plated onto 20 Petri dishes at a seeding density of 3 × 10⁶ cells/plate and cultured in DMEM, 10% FBS, and 1% Pen/Strep. The day after, cells were co-transfected by the calcium-phosphate method. Each plate was transfected with 13 μg of pLV-SIN-EGFP, 13 μg of pCMVΔ8.92, 3 μg of pRSV-Rev, and 3.75 μg of pMDG. After 16 h, fresh medium was added and cells were cultured for a further 48 h before supernatant collection. The virus-containing medium was then filtered through a 0.45-μm filter to remove cells and debris, and a high-titer viral preparation was achieved by ultracentrifugation at 68,580 × g for 90 min at 4°C. The virus was resuspended over several hours on ice in 1% BSA in PBS, aliquoted, and stored at –80°C until use.

Vector titration (TU) was performed on HeLa cells with flow cytometry. TU was calculated by quantifying the number of EGFP-positive HeLa cells after transduction with serial dilutions (10⁻², 10⁻³, and 10⁻⁴ μL of vector) of the concentrated lentivirus preparation. Viral titer was calculated as transduction units per milliliter (TU/mL) using the volume of virus used for infection.

Lentivirus transduction of ADSCs and long-term cell storage

In order to estimate the optimal titer that would lead to high transduction efficiency and low toxicity, we performed a dose-response experiment by infecting ADSCs with viral particles at a multiplicity of infection (MOI) of 10, 40, 80, and 100 in the presence or absence of 4 μg/mL polybrene (Sigma, St. Louis, MO, USA). Passage 2 ADSCs were seeded at a density of 7,000 cells/cm² in 12-well plates and incubated under standard culture conditions for 16 h. Cells were then transduced for 7 h with a final volume of 0.5 mL/well of virus before addition of another 0.5 mL/well of fresh complete medium. After 24 h, lentivirus-containing medium was replaced with fresh medium and cells were left in the incubator for 72 h. Transduction efficiency and cell morphology were monitored daily by fluorescent microscopy before quantification by flow cytometry analysis on PFA-fixed cells.

The MOI of 40 in the presence of 4 µg/mL polybrene was used in the following experiments, as nearly 99% of the cells were positive for GFP and cell morphology was similar to the non-transduced ADSCs.

After lentivirus infection, passage 2 EGFP-ADSCs were grown to 80% confluence and collected for long-term cell storage. Briefly, cells were lifted with trypsin, washed in PBS by centrifugation, and resuspended in freezing medium consisting of 80% FBS (Gibco, Waltham, MA, USA), 10% DMEM (Lonza, Basel, Switzerland), and 10% dimethyl sulfoxide (DMSO) (Sigma, St. Louis, MO, USA) at a concentration of 1 million cells per milliliter of cryopreservation medium. Cells were then aliquoted in cryovials, placed in an isopropanol freezing container, and frozen at -80°C . After 24 h, cryovials were transferred in liquid nitrogen.

To revive EGFP-ADSCs, cells were rapidly thawed at 37°C , washed in complete medium by centrifugation, and plated at a concentration of 1×10^4 cells/cm². EGFP-ADSCs were then grown for one more passage before being characterized by flow cytometry and multidifferentiation potential.

Animal experiments

All experiments involving mice were conducted in accordance with the Animals (Scientific Procedures) Act 1986 under a UK Home Office project license approved by the Sheffield University Ethical Review Committee Project Applications and Amendments Subcommittee and by the UK Animal Procedures Committee (London, UK). The mouse colony was maintained in a specific pathogen-free (SPF) environment before being moved for experiments to a conventional animal facility following the Home Office code of practice for the housing and care of animals used in scientific procedures (12-h light/dark cycle and RT maintained at 21°C). Each mouse cage floor was covered with a layer of fine sawdust (Eco-Pure Flakes 6, Datesand, UK) and contained a plastic house and paper wool (Datesand, UK). Female mice from the same litter were housed together in pairs, triplets, or quadruplets, and rodent diet (Harlan, UK) and water were provided *ad libitum*. Transgenic C57BL/6J-Tg (SOD1^{G93A})1Gur/J mice of the defined C57BL/6J-OlaHsd inbred genetic background were used in this study.³³ Since there are no significant differences in disease progression between males and females in our model,³³ hemizygous transgenic males were bred with wild-type females to maintain the SOD1^{G93A} transgene, while hemizygous females were used for experiments. Transgenic SOD1^{G93A} mice were identified by PCR amplification of genomic DNA extracted from ear tissue with QuickExtract DNA Extraction Solution 1.0 (Lucigen, Middleton, WI, USA). DNA amplification was performed in a 10-µL volume of 5× FIREPol Master Mix Ready to Load (Solis Biodyne, Tartu, Estonia) and 10 nm of each of the human SOD1 primers (forward 5'-CATCAGCCCTAATCCATCTGA-3', reverse 5'-CGCGACTAA CAATCAAAGTGA-3') and mouse IL-2R primers (forward 5'-CTA GGCCACAGAATTGAAAGATCT-3', reverse 5'-GTAGGTGGAA ATTCTAGCATCATC-3'). Electrophoresis was performed on a 2% agarose gel, and bands were visualized at 324 bp for IL-2R and 236 bp for hSOD1 when present.

For the *in vivo* therapeutic study, we followed the recommendations for the conduct of pre-clinical studies in the SOD1^{G93A} mouse model released by the ALS Therapy Development Institute (ALS TDI), which were successively updated in 2009 following an international conference held in Germany, 11–13 June 2009.⁷⁴ To determine group size, a statistical power analysis using G*Power 3.1. was carried out.⁷⁵ This ensured reduction in the number of animals used in the experiment to a minimum, in compliance with the guideline on the principles of regulatory acceptance of 3Rs testing approaches.⁷⁶ Power analysis was performed based on the detection of a 10-day shift in the time taken to reach a 20% decline in rotarod performance. A power of 80% was used with a two-tailed Student's t test ($\alpha = 0.05$, $\beta = 0.8$). The analysis indicated that 14 mice per group are required to detect a 10-day difference in time taken to reach the rotarod decline. The group size was finally increased by 1 ($n = 15$) in order to account for unexpected (unrelated health problems) loss of animals.

Intrathecal transplantation of EGFP-ADSCs via cisterna magna

EGFP-ADSCs were thawed from frozen stocks and cultured for 4–5 days before being used for transplantation. When cultures reached 80% confluence, cells were detached by trypsinization, washed in PBS, counted, and resuspended in 200 µL of HypoThermosol FRS solution (BioLife Solutions, Bothell, WA, USA) and stored at 4°C until ready to be transplanted. Cells were transplanted into the CSF of mice through cisterna magna injection. The surgical procedure was adapted from previous studies.⁷⁷ Before surgery, mice were placed in an induction chamber and anesthetized with 5% isoflurane (5 mL/min). Unconscious mice were then shaved and placed prone on a heat pad, and the head was fixed, with the help of a tooth and ear bars, to a stereotaxic apparatus. During surgery deep anesthesia was maintained with isoflurane 1%–2% (2 mL/min). To expose the atlanto-occipital membrane, the skin was incised from the nuchal line to the level of the second/third cervical vertebrae and the muscles separated by blunt dissection. To keep the muscles apart, a pair of micro-retractors were used. After exposure of the atlanto-occipital membrane, EGFP-ADSCs were prepared for transplantation. Cells were spun at $366 \times g$ for 4 min and re-suspended in sterile RT PBS at a concentration of 50,000 cells/µL. For injection, cells were taken into a Hamilton syringe (702 RN 25 µL) (Hamilton, Reno, NV, USA). The syringe was then placed in a standard infuse/withdraw programmable syringe pump (Harvard Apparatus 350, Cambridge, UK) connected to the micromanipulator on the stereotaxic apparatus. The needle (Gauge 31, point style 4 at 45°) was carefully directed toward the midline of the atlanto-occipital membrane, the dura mater was pierced, and the needle was withdrawn to allow outflow of CSF. The needle was then moved forward and stopped 1 mm inside the cisterna magna. A total of 10 µL of cell suspension corresponding to 500,000 cells was injected at a rate of 1 µL/min. At the end of the injection, the needle was kept in place for a further 10 min to avoid cell leakage and then slowly withdrawn. The dorsal muscles were sutured with absorbable 5-0 Vicryl (Ethicon, Somerville, NJ, USA) and the skin with non-absorbable nylon monofilament (Ethicon, Somerville, NJ, USA). The mouse was then moved in an incubator set at 28°C until complete recovery. Mice were able to walk normally

15 - 25 min post-surgery. For the vehicle group, mice were injected with 10 μ L of sterile PBS.

Behavior tests

Weight was measured twice per week in the afternoon immediately prior to the rotarod test. The rotarod test was carried out for a maximum period of 300 s, with the rotarod (Ugo Basile 7650, Gemonio, Italy) set to accelerate from 4 to 40 rpm in 270 s. On each testing day, mice were tested twice, with a rest period of 3 min in between tests, and latency to fall was recorded in seconds. The highest score was used for analysis. The first rotarod testing day started at the age of 30–32 days after the mice received training for 3 consecutive days. In order to determine rotarod decline, the best score among the first test and the three training tests was used as peak of performance. Rotarod performance was carried out until the end of the study. Gait parameters were captured with the CatWalk gait system (Noldus Instruments 7.1, Nottingham, UK) in groups of 5 \times SOD1^{G93A} transgenic mice (ADSC-injected and PBS-injected mice) at 70 and 84 days of age. Mice were placed on the CatWalk apparatus in complete darkness and allowed to walk without interference. At least 6 straight and continuous runs were recorded, and the 3 straightest runs were selected for analysis. Gait data were analyzed with the dedicated CatWalk software (version 7.1). Each paw print was labeled manually, followed by automatic detection of gait parameters. Neurological deficit scoring was performed in the afternoon every 3 days from 60 days of age onward with a system previously described in the literature.³³ Forelimb and hindlimb tremors were individually scored based on a scale of 0–3 (0 - normal, 1 - mild, 2 - moderate, 3 - strong) during mouse suspension by the tail. At the same time, hindlimb splay defects were evaluated individually for left and right limbs on a scale of 0–4 (0 - normal, 1 - mild, 2 - moderate, 3 - strong, 4 - paralyzed). The neurological deficit was delineated by an overall score (0 - normal, 0.5 - onset, 1 - abnormal gait, 2 - severe waddle, 3 - dragging one hindlimb, 4 - paralysis of one limb) and onset of disease defined by co-existing hindlimb splay defect and hindlimb tremor for two consecutive tests. All behavioral tests were performed by the same investigator, who was blinded to the treatment group.

Tissue collection and processing for engraftment qualitative studies

Mice were sacrificed with an anesthetic overdose by intraperitoneal injection of pentobarbitone (2.5 mL/kg) and perfused with 7.5 mL of cold PBS, followed by 20 mL of 2% PFA in PBS. The whole skull and vertebral column were post-fixed in 2% PFA at 4°C O/N. The following day, dissection of whole CNS with intact dura mater was performed under the microscope. The dissection protocol was adapted from the literature.³² After extraction of the brain from the skull and spinal cord from the column, tissue was cryoprotected by immersion in 20% sucrose (Sigma, St. Louis, MO, USA) in PBS at 4°C O/N. The spinal cord was then sectioned into cervical, thoracic, and lumbar segments and the brain dissected into forebrain, midbrain, and hindbrain. Tissue was finally frozen in OCT medium (CellPath Ltd, Newtown, UK) over methanol/dry ice and stored at –80°C.

Samples were sectioned at 20- μ m thickness with the use of a cryostat and mounted on uncoated glass slides. Slides were dried at 37°C for 30 min, washed in PBS with gentle agitation (3 \times 10 min) at RT, and finally mounted in Vectashield aqueous hard-set mounting containing 4',6-diamidino-2-phenylindole (DAPI) (VectaLabs, Burlingame, CA, USA). Slides were left to air-dry in the dark at RT O/N. Images were captured with an IN Cell 2000 analyzer (GE Healthcare, Chicago, IL, USA).

Immunohistochemistry

Under terminal anesthesia, mice were perfused with 8 mL of ice-cold PBS followed by perfusion with 10 mL of ice-cold 4% PFA. The spinal column was collected and post-fixed O/N in 4% PFA/PBS at 4°C. The following day, the spinal cord was dissected from the column, washed in PBS, and divided into cervical, thoracic, and lumbar segments. The lumbar enlargement (12 mm) was cut in half and embedded in paraffin within a single block with the two median extremities oriented upward. Tissue was then sliced at 10- μ m thickness with a microtome. Sections were mounted serially over series of 5 slides, with 5 sections being discarded in between series, for a total of 60 slides covering 4.8 mm of spinal cord tissue. This ensured that there was a distance of at least 100 μ m between serial sections. Each slide contained 8 sections. Sections were rehydrated by immersion in alcohol gradients using the following sequence: 2 \times 5 min in xylene, 5 min in 100% ethanol, 5 min in 95% ethanol, 5 min in 70% ethanol, and 5 min in water. After deparaffinization, heat-induced epitope retrieval was performed. Slides were completely submerged in Access Super RTU pH 8 (Menarini, Florence, Italy) and placed in an antigen access unit (Menarini, Florence, Italy) for 30 min at 125°C with a pressure of 20 psi. At the end of the cycle, slides were left to cool at RT and washed in PBS for 10 min with gentle agitation. Sections were then blocked/permeabilized for 20 min at RT with 5% BSA, 0.25% Triton X-100 (Sigma, St. Louis, MO, USA) in PBS. After blocking/permeabilization, slides were co-immunostained for mouse GFAP (chicken polyclonal, 1:500) (Abcam, Cambridge, UK) and for mouse Iba1 (rabbit polyclonal, 1:500) (GeneTex, Irvine, CA, USA) diluted in 1% BSA, 0.25% Triton X-100/PBS at 4°C O/N. Slides were then given 6 quick washes and 3 \times 8 min washes in PBS, blocked in 5% BSA/PBS for 10 min at RT, and incubated with the secondary antibodies conjugated to Alexa Fluor 488 (1:1,000) (Thermo Fisher, Waltham, MA, USA) or Alexa Fluor 555 (1:1,000) Thermo Fisher, Waltham, MA, USA) at RT for 90 min. After incubation, slides were washed with 2 quick washes in PBS, 4 \times 8 min washes in PBS, and 1 \times 5 min wash in distilled water in the dark. Slides were dried to remove water excess, mounted with Vectashield hard set aqueous solution with DAPI (VectaLabs, Burlingame, CA, USA), and left to dry at RT O/N in the dark. Images were captured with the IN Cell 2000 analyzer (GE Healthcare, Chicago, IL, USA) and analyzed with the GE Developer Toolbox 1.9 (GE Healthcare, Chicago, IL, USA). GFAP and Iba1 staining was captured within each ventral horn of each spinal cord section (8 sections/mouse) at a magnification of 60 \times . GFAP staining was segmented by intensity level with a threshold greater than 220 gray levels, followed by a sieve filter over 4 μ m. Total staining area (μ m²) and main staining index [(unstained pixels – stained pixels)/2 \times SD] were recorded. Iba1

staining was segmented by intensity level with a threshold greater than 200 gray levels, followed by a sieve filter over 4 μm . Total staining area (μm^2) was recorded.

Nissl staining and motor neuron counts

Paraffin serial sections of lumbar spinal cord were processed for Nissl staining. The staining was performed on every 5th section (total of 12 slides per mouse with 8 sections per slide) covering a total length of ~ 4.8 mm of the lumbar spinal cord, with at least 100 μm of space between each section. Nissl staining was performed according to the literature. Briefly, sections were dewaxed in xylene, rehydrated through graded alcohols, and stained with pre-filtered 0.1% cresyl fast violet for 20 min. Sections were then rinsed quickly in distilled water and differentiated in 0.25% ethanoic acid for 10 s. After washing in distilled water, sections were dehydrated by immersion baths in crescent graded alcohols with the following sequence: 5 min in 70% ethanol, 5 min in 95% ethanol, 2 \times 5 min in 100% ethanol, and 5 min in xylene to clear. Slides were dried, mounted in permanent mounting medium (H-5000, VectaMount), and dried at 37°C O/N.

Nissl-positive α -MNs were identified and counted depending on their topography, morphology, and size. α -MNs were defined as multipolar cells located in the ventral horn of the lumbar spinal cord, characterized by the presence of a large nucleus with intensely labeled nucleoli and a diameter size of at least 25 μm . A total of 96 sections (192 ventral horns) were screened for each mouse ($n = 6$ per group). MN counting was performed by the same investigator, who was blinded to the treatment group.

Isolation and culture of mouse cortical astrocytes

Mouse cortical astrocytes were isolated from symptomatic (90 days) female transgenic SOD1^{G93A} and control sex- and age-matched NTg mice. Isolation and culture of astrocytes was performed as previously described with minor modifications.⁷⁸ Mice were sacrificed by cervical dislocation, and brains from 3 mice were isolated and pooled together. Cerebellum and meninges were carefully dissected, and tissue was digested with papain (200 U/mL) (Sigma, St. Louis, MO, USA) diluted in enzymatic buffer (116 mM NaCl, 5.4 mM KCl, 26 mM NaHCO₃, 1 mM NaH₂PO₄, 1.5 mM CaCl₂, 1 mM MgSO₄, 25 mM glucose, 1 mM cysteine in ddH₂O). After DNase treatment and mechanical dissociation, tissue homogenate was filtered through a 70- μm cell strainer and cell isolated by density gradient using 20% Percoll solution (Sigma, St. Louis, MO, USA). The cell pellet was re-suspended in complete astrocyte medium (DMEM) (Fisher Scientific, Hampton, NH, USA), 10% FBS (Life Science Production, Bedford, UK), and 1% Pen/Strep (Gibco, Waltham, MA, USA) and plated in a standard culture flask previously pre-coated with 0.01% poly-L-ornithine (Sigma, St. Louis, MO, USA). Cells were grown in an incubator at 37°C with 20% O₂, 5% CO₂ and 95% humidity. Medium was replaced every 3 days for ~ 14 days. When cultures reached confluence, flasks were placed on an orbital shaker at 230 rpm, 37°C for 12 h to remove contaminating microglia. mAstrocytes were then detached with mild trypsinization and expanded.⁷⁹ For these experiments, mAstrocytes were used at passage 4.

Reprogramming of human fibroblasts into neural progenitor cells (iNPCs)

Skin biopsy collection from ALS patients and healthy donors (Table S1) was approved by the Research Ethics Committee of Sheffield (study number STH16573, reference 12/YH/0330) or by the Institutional Review Board of the Ohio State University (ethics number IRB08-00402) after informed consent was obtained.

Fibroblasts from 2 non-ALS control subjects and 2 C9orf72, 2 SOD1^{A4V}, and 2 sporadic ALS patients were reprogrammed into neural progenitor cells (induced NPCs [iNPCs]) as previously described.³⁰ Fibroblasts were grown into one well of a six-well plate for 24 h before being transduced with retroviral vectors expressing Oct4, Sox 2, Klf 4, and c-Myc. Cells were allowed to recover for 1 day in basal fibroblast medium composed of DMEM (Gibco, Waltham, MA, USA) and 10% FBS (Life Science Production, Bedford, UK) and switched to NPC conversion medium consisting of DMEM/F12 (1:1) GlutaMax (Gibco, Waltham, MA, USA), 1% N2 (Gibco, Waltham, MA, USA), 1% B27 (Gibco, Waltham, MA, USA), 20 ng/mL FGF2 (PeproTech, Rocky Hill, NJ, USA), 20 ng/mL EGF (PeproTech, Rocky Hill, NJ, USA), and 5 ng/mL heparin (Sigma, St. Louis, MO, USA). After morphology changes, rosette-like structures were switched to NPC proliferation medium consisting of DMEM/F12 (1:1) GlutaMax, 1% N2, 1% B27, and 40 ng/mL FGF2, where iNPCs were expanded.

Differentiation of iNPCs into iAstrocytes

iAstrocytes were obtained as previously described.³⁰ iNPCs were seeded in 10-cm dishes coated with fibronectin and induced to differentiate for 7 days by culture in astrocyte proliferation medium composed of DMEM (Fisher Scientific, Hampton, NH, USA) containing 10% FBS (Life Science Production, Bedford, UK) and 0.2% N2 (Gibco, Waltham, MA, USA).

Hb9-EGFP motor neurons

Murine Hb9-EGFP MNs were obtained from mESCs containing an EGFP gene under the MN-specific promoter Hb9 (kind gift from Thomas Jessell, Columbia University, New York, NY, USA). Hb9-EGFP mESCs were differentiated as previously described.⁸⁰ At the end of the differentiation (7 days), the Hb9-EGFP MN enriched fraction was obtained by embryo body dissociation with 20 U/mL papain (Sigma, St. Louis, MO, USA) as previously described.⁸¹

Hb9-EGFP-MN, mouse astrocyte, and ADSC separated co-cultures

For co-culture experiments, three separated astrocyte preparations per genotype (SOD1^{G93A} and NTg) were established (biological replicates). Passage 4 mAstrocytes from symptomatic (90 day old) SOD1^{G93A} or NTg age-matched control mice were seeded in triplicate (technical replicate) onto 1 well of a 24-well plate previously coated with 1:1,000 poly-L-ornithine (Sigma, St. Louis, MO, USA) and laminin 1:200 (Sigma, St. Louis, MO, USA), at a concentration of 50,000 cells/well. mAstrocytes were maintained for 24 h in astrocyte basal medium (DMEM, 10% FBS, 1% Pen/Strep). On the same day,

30,000 passage 5 ADSCs were plated onto sterile glass coverslips (22 mm²) containing 2-mm² paraffin wax dots. The next day, the Hb9-EGFP MN enriched fraction was obtained and 30,000 cells/well were plated onto the mAstrocyte monolayer in 1 mL of MN medium consisting of KnockOut DMEM, F12 medium, 10% KnockOut Serum Replacement, 1 mM L-glutamine, 0.5% (w/v) glucose, 1% N2, 0.0016% (v/v) 2-mercaptoethanol, 20 ng/mL brain-derived neurotrophic factor (BDNF) (PeproTech, Rocky Hill, NJ, USA), 40 ng/mL ciliary neurotrophic factor (CNTF) (PeproTech, Rocky Hill, NJ, USA), and 20 ng/mL glial cell-derived neurotrophic factor (GDNF) (PeproTech, Rocky Hill, NJ, USA). Before addition of the MN, the astrocyte medium was removed and astrocytes washed with PBS. After 5 h, each coverslip containing the ADSCs was washed in PBS and laid onto the astrocyte/Hb9-EGFP MN mixed co-culture. Thus, ADSCs were only physically separated from astrocytes and MNs. Every alternate day, 500 µL of medium was replaced with fresh complete MN medium until day 7 of co-culture. Hb9-EGFP MNs were imaged with the IN Cell 2000 analyzer (GE Healthcare, Chicago, IL, USA) 24 h after the initiation of the co-culture to measure the number of cells at day 1. Plates were then imaged at day 7. The number of viable MNs was counted with the Columbus Data Storage and Analysis System (RRID:SCR_007149; Perkin Elmer, Waltham, MA, USA). Only GFP-positive motor neuronal cell bodies with at least 2 cell processes were counted as viable cells. Finally, the percentage of MN survival was calculated as the number of viable MNs at day 7 as a percentage of the number of viable MNs at day 1.

Hb9-EGFP MN, human iAstrocyte, and ADSC separated co-cultures

Human iAstrocytes were grown in 10-cm dishes in complete iAstrocyte proliferation medium (DMEM, 10% FBS, 0.2% N2). At day 6 of differentiation, cells were lifted with Accutase and plated in quintuplicate into one well of a 24-well plate coated with 1:400 fibronectin. Cells were seeded at a concentration between 10,000 and 40,000 cells/well depending on the cell line. ADSCs were plated onto glass coverslips (22 mm²) containing paraffin wax dots at a concentration of 30,000 cells/well. After 24 h (day 7 for iAstrocyte differentiation), 40,000 Hb9-EGFP MNs were seeded on top of the iAstrocytes and medium was switched to MN medium (KnockOut DMEM, F12 medium, 10% KnockOut Serum Replacement, 1 mM L-glutamine, 0.5% (w/v) glucose, 1% N2, 0.0016% (v/v) 2-mercaptoethanol, 20 ng/mL BDNF, 40 ng/mL CNTF, and 20 ng/mL GDNF). After 5 h, the coverslips containing ADSCs were flipped over the iAstrocytes/MN mixed co-culture to obtain the triple-separated co-culture. The following day, plates were imaged with the IN Cell 2000 analyzer (GE Healthcare, Chicago, IL, USA) for quantification of viable MNs at day 1. Hb9-EGFP MNs were imaged again at day 3 and the percentage of MN survival calculated as viable cells at day 3 as a percentage of viable MNs at day 1.

Mouse astrocyte and ADSC separated co-cultures

mAstrocytes derived from SOD1^{G93A} and age-matched NTg mice obtained from three separate preparations were plated onto 24-well plates coated with 1:1,000 poly-L-ornithine (A-004-C,

Sigma-Aldrich) at a concentration of 50,000 cells per well. mAstrocytes were allowed to recover for 2 days before addition of 30,000 ADSCs/well previously seeded onto glass coverslips containing wax dots. Separated co-cultures were maintained for 48 h in complete mAstrocyte medium (DMEM, 10% FBS, 1% Pen/Strep). Empty coverslips were used as a negative control. At the end of the co-culture period, for supernatant protein analysis, the coverslips containing ADSCs were removed, washed in PBS, and cultured for a further 24 h in 500 µL of control serum-free medium. mAstrocyte cultures were also washed in PBS twice, and 300 µL of fresh serum-free medium was added. After 24 h, the supernatant from both astrocytes and ADSCs was collected, spun at 600 × g at 4°C for 10 min, and snap frozen in liquid nitrogen. Samples were stored at –80°C until ready to use. After supernatant collection, mAstrocytes were fixed with 4% PFA (v/v) in PBS for 10 min and stained with Hoechst 33342 Solution (62249, Thermo Fisher Scientific) diluted 1:5,000. Plates were then imaged with the IN Cell 2000 analyzer (GE Healthcare) and cell nuclei counted with the Columbus Data Storage and Analysis System (RRID:SCR_007149; Perkin Elmer, Waltham, MA, USA).

Multiplex bead-based immunoassay

Soluble cytokines in supernatants were measured with the use of the BD Cytometric Bead Array (CBA) Flex Set multiplexed bead-based immunoassay (BD Biosciences), which allows up to 30 analytes to be measured simultaneously. Samples were analyzed for IL-6, IL-1β, TNF-α, and MCP-1. The assay was performed according to the manufacturer's instructions, and samples were acquired on an Attune dual-laser flow cytometer (Thermo Fisher, Waltham, MA, USA). The data files were collected as Excel sheets and analyzed with GraphPad 7. First, a nonlinear regression standard curve (Curve Fit) was generated. This was then used to extrapolate the sample values. Protein concentration (pg/mL or pg/mL) for each well/sample was finally normalized to the number of cells counted at the end of the experiment in that specific well.

ELISA

VEGF-A and IGF-1 protein concentrations in the supernatant collected from mAstrocytes and ADSCs after separated co-culture were quantified by sandwich enzyme-linked immunosorbent assay (ELISA) using commercial ELISA kits.

For VEGF-A measurement, the mouse VEGF-A Platinum ELISA kit (BMS619/2, Thermo Fisher Scientific) was used according to the manufacturer's instruction. IGF-1 protein concentration was quantified with the mouse IGF-1 ELISA Kit (EMIGF1, Thermo Fisher Scientific) according to the manufacturer's instructions. Before starting the protocol, samples stored at –80° were thawed on ice and diluted with the assay diluent provided in the kit. The standard and each sample were loaded in duplicate into the specific antibody-pre-coated 96-well strip plate provided in the kit and the manual instructions followed. At the end of the protocol, absorbance was read at 450 nm with the PHERAStar microplate reader (BMG, Labtech) and absorbance values transferred to an Excel data sheet. Data were finally analyzed

with GraphPad 7. Briefly, the optical density value from the control (medium alone) was subtracted from the standard and sample readings. Data were then plotted on GraphPad 7, and a nonlinear sigmoidal standard curve (Curve Fit) was fitted. Protein concentration in the samples was then extrapolated and normalized to the number of cells counted at the end of the co-culture.

Statistical analysis

All statistical analyses were performed with GraphPad Prism 7 (GraphPad, San Diego, CA, USA). The 1-way ANOVA with Tukey's multiple comparison test, 2-way ANOVA with Sidak's multiple comparison test, 2-way ANOVA with Bonferroni post hoc test, Student's *t* test, or Mann-Whitney *U* test was used depending on the number of variables in each experiment. Statistical significance was considered with a *p* < 0.05.

SUPPLEMENTAL INFORMATION

Supplemental information can be found online at <https://doi.org/10.1016/j.omtm.2021.03.017>.

ACKNOWLEDGMENTS

This work was supported by a University of Sheffield PhD scholarship awarded to Y.C. and the NIHR Sheffield Biomedical Research Centre (IS-BRC-1215-20017). R.J.M. was supported by a tenure track Lectureship awarded by the Motor Neurone Disease Association and the family of Kenneth A. Snowman (SITraN/Apr13/983-797). P.J.S. is supported as an NIHR Senior Investigator (NF-SI-0617-10077). L.F. is supported by the Academy of Medical Sciences (SBF002\1142) and the Medical Research Council (MRC; grant 1812144). The views expressed are those of the authors and not necessarily those of the NHS, the NIHR, or the Department of Health and Social Care (DHSC). The authors would like to acknowledge the technical assistance of staff in the Biological Services Unit at the University of Sheffield and the Sheffield Institute for Translational Neuroscience, particularly Ian Coldicott. We are grateful to M. Stopford, M. Myszczyńska, N. Markus, and A. Varciana for iAstrocyte production and Hb9-EGFP-MN differentiation; E. Karika for assisting in lentivirus production; and A. Higginbottom for technical assistance. We also thank the Flow Cytometry Core Service at the University of Sheffield for technical assistance. We are very grateful to the ALS patients and control subjects who generously donated the fibroblasts used in this study.

AUTHOR CONTRIBUTIONS

R.J.M., P.J.S., and Y.C. assisted in the planning and conception of all experiments, L.F. assisted in the planning and conception of astrocyte/motor neuron co-culture experiments, A.G. assisted in the planning and conception of *in vivo* transplantation experiments, N.G. contributed to the *in vitro* experiments involving iAstrocytes, and C.A. contributed to the *in vitro* experiments involving Hb9-EGFP-MNs. Y.C. conducted the experiments, performed data analysis, and drafted the manuscript and figures. R.J.M., P.J.S., L.F., and A.G. critically appraised the data and edited the manuscript. All authors read and approved the final manuscript.

DECLARATION OF INTERESTS

The authors declare no competing interests.

REFERENCES

- Hardiman, O., Al-Chalabi, A., Chio, A., Corr, E.M., Logroscino, G., Robberecht, W., Shaw, P.J., Simmons, Z., and van den Berg, L.H. (2017). Amyotrophic lateral sclerosis. *Nat. Rev. Dis. Primers* 3, 17071.
- Brown, R.H., and Al-Chalabi, A. (2017). Amyotrophic Lateral Sclerosis. *N. Engl. J. Med.* 377, 162–172.
- Taylor, J.P., Brown, R.H., Jr., and Cleveland, D.W. (2016). Decoding ALS: from genes to mechanism. *Nature* 539, 197–206.
- Mead, R.J., Higginbottom, A., Allen, S.P., Kirby, J., Bennett, E., Barber, S.C., Heath, P.R., Coluccia, A., Patel, N., Gardner, I., et al. (2013). S[+] Apomorphine is a CNS penetrating activator of the Nrf2-ARE pathway with activity in mouse and patient fibroblast models of amyotrophic lateral sclerosis. *Free Radic. Biol. Med.* 61, 438–452.
- Cleveland, D.W., Bruijn, L.I., Wong, P.C., Marszalek, J.R., Vecchio, J.D., Lee, M.K., Xu, X.S., Borchelt, D.R., Sisodia, S.S., and Price, D.L. (1996). Mechanisms of selective motor neuron death in transgenic mouse models of motor neuron disease. *Neurology* 47 (4, Suppl 2), S54–S61, discussion S61–S62.
- Smith, E.F., Shaw, P.J., and De Vos, K.J. (2019). The role of mitochondria in amyotrophic lateral sclerosis. *Neurosci. Lett.* 710, 132933.
- Van Den Bosch, L., Van Damme, P., Bogaert, E., and Robberecht, W. (2006). The role of excitotoxicity in the pathogenesis of amyotrophic lateral sclerosis. *Biochim. Biophys. Acta* 1762, 1068–1082.
- Barber, S.C., and Shaw, P.J. (2010). Oxidative stress in ALS: key role in motor neuron injury and therapeutic target. *Free Radic. Biol. Med.* 48, 629–641.
- Donnelly, C.J., Zhang, P.W., Pham, J.T., Haeusler, A.R., Mistry, N.A., Vidensky, S., Daley, E.L., Poth, E.M., Hoover, B., Fines, D.M., et al. (2013). RNA toxicity from the ALS/FTD C9ORF72 expansion is mitigated by antisense intervention. *Neuron* 80, 415–428.
- Boillée, S., Yamanaka, K., Lobsiger, C.S., Copeland, N.G., Jenkins, N.A., Kassiotis, G., Kollias, G., and Cleveland, D.W. (2006). Onset and progression in inherited ALS determined by motor neurons and microglia. *Science* 312, 1389–1392.
- Di Giorgio, F.P., Boulting, G.L., Bobrowicz, S., and Eggan, K.C. (2008). Human embryonic stem cell-derived motor neurons are sensitive to the toxic effect of glial cells carrying an ALS-causing mutation. *Cell Stem Cell* 3, 637–648.
- Yamanaka, K., and Komine, O. (2018). The multi-dimensional roles of astrocytes in ALS. *Neurosci. Res.* 126, 31–38.
- Frakes, A.E., Braun, L., Ferraiuolo, L., Guttridge, D.C., and Kaspar, B.K. (2017). Additive amelioration of ALS by co-targeting independent pathogenic mechanisms. *Ann. Clin. Transl. Neurol.* 4, 76–86.
- Ciervo, Y., Ning, K., Jun, X., Shaw, P.J., and Mead, R.J. (2017). Advances, challenges and future directions for stem cell therapy in amyotrophic lateral sclerosis. *Mol. Neurodegener.* 12, 85.
- Baloh, R.H., Glass, J.D., and Svendsen, C.N. (2018). Stem cell transplantation for amyotrophic lateral sclerosis. *Curr. Opin. Neurol.* 31, 655–661.
- Boido, M., Piras, A., Valsecchi, V., Spigolon, G., Mareschi, K., Ferrero, I., Vizzini, A., Temi, S., Mazzini, L., Fagioli, F., and Vercelli, A. (2014). Human mesenchymal stromal cell transplantation modulates neuroinflammatory milieu in a mouse model of amyotrophic lateral sclerosis. *Cytotherapy* 16, 1059–1072.
- Boucherie, C., Schäfer, S., Lavand'homme, P., Maloteaux, J.M., and Hermans, E. (2009). Chimerization of astroglial population in the lumbar spinal cord after mesenchymal stem cell transplantation prolongs survival in a rat model of amyotrophic lateral sclerosis. *J. Neurosci. Res.* 87, 2034–2046.
- Kim, H., Kim, H.Y., Choi, M.R., Hwang, S., Nam, K.H., Kim, H.C., Han, J.S., Kim, K.S., Yoon, H.S., and Kim, S.H. (2010). Dose-dependent efficacy of ALS-human mesenchymal stem cells transplantation into cisterna magna in SOD1-G93A ALS mice. *Neurosci. Lett.* 468, 190–194.
- Zhou, C., Zhang, C., Zhao, R., Chi, S., Ge, P., and Zhang, C. (2013). Human marrow stromal cells reduce microglial activation to protect motor neurons in a transgenic mouse model of amyotrophic lateral sclerosis. *J. Neuroinflammation* 10, 52.

20. Sironi, F., Vallarola, A., Violatto, M.B., Talamini, L., Freschi, M., De Gioia, R., Capelli, C., Agostini, A., Moscatelli, D., Tortarolo, M., et al. (2017). Multiple intracerebroventricular injections of human umbilical cord mesenchymal stem cells delay motor neurons loss but not disease progression of SOD1G93A mice. *Stem Cell Res. (Amst.)* 25, 166–178.
21. Romanov, Y.A., Svintsitskaya, V.A., and Smirnov, V.N. (2003). Searching for alternative sources of postnatal human mesenchymal stem cells: candidate MSC-like cells from umbilical cord. *Stem Cells* 21, 105–110.
22. Marconi, S., Bonaconca, M., Scambi, I., Squintani, G.M., Rui, W., Turano, E., Ungaro, D., D'Agostino, S., Barbieri, F., Angiari, S., et al. (2013). Systemic treatment with adipose-derived mesenchymal stem cells ameliorates clinical and pathological features in the amyotrophic lateral sclerosis murine model. *Neuroscience* 248, 333–343.
23. Kim, K.S., Lee, H.J., An, J., Kim, Y.B., Ra, J.C., Lim, I., and Kim, S.U. (2014). Transplantation of human adipose tissue-derived stem cells delays clinical onset and prolongs life span in ALS mouse model. *Cell Transplant.* 23, 1585–1597.
24. Zuk, P.A., Zhu, M., Mizuno, H., Huang, J., Futrell, J.W., Katz, A.J., Benhaim, P., Lorenz, H.P., and Hedrick, M.H. (2001). Multilineage cells from human adipose tissue: implications for cell-based therapies. *Tissue Eng.* 7, 211–228.
25. Baglioni, S., Francalanci, M., Squecco, R., Lombardi, A., Cantini, G., Angeli, R., Gelmini, S., Guasti, D., Benvenuti, S., Annunziato, F., et al. (2009). Characterization of human adult stem-cell populations isolated from visceral and subcutaneous adipose tissue. *FASEB J.* 23, 3494–3505.
26. Meyer, J., Salamon, A., Herzmann, N., Adam, S., Kleine, H.D., Matthiesen, I., Ueberreiter, K., and Peters, K. (2015). Isolation and differentiation potential of human mesenchymal stem cells from adipose tissue harvested by water jet-assisted liposuction. *Aesthet. Surg. J.* 35, 1030–1039.
27. Han, C., Zhang, L., Song, L., Liu, Y., Zou, W., Piao, H., and Liu, J. (2014). Human adipose-derived mesenchymal stem cells: a better cell source for nervous system regeneration. *Chin. Med. J. (Engl.)* 127, 329–337.
28. Ferraiuolo, L., Higginbottom, A., Heath, P.R., Barber, S., Greenald, D., Kirby, J., and Shaw, P.J. (2011). Dysregulation of astrocyte-motoneuron cross-talk in mutant superoxide dismutase 1-related amyotrophic lateral sclerosis. *Brain* 134, 2627–2641.
29. Haidet-Phillips, A.M., Hester, M.E., Miranda, C.J., Meyer, K., Braun, L., Frakes, A., Song, S., Likhite, S., Murtha, M.J., Foust, K.D., et al. (2011). Astrocytes from familial and sporadic ALS patients are toxic to motor neurons. *Nat. Biotechnol.* 29, 824–828.
30. Meyer, K., Ferraiuolo, L., Miranda, C.J., Likhite, S., McElroy, S., Renusch, S., Ditsworth, D., Lagier-Tourenne, C., Smith, R.A., Ravits, J., et al. (2014). Direct conversion of patient fibroblasts demonstrates non-cell autonomous toxicity of astrocytes to motor neurons in familial and sporadic ALS. *Proc. Natl. Acad. Sci. USA* 111, 829–832.
31. Bourin, P., Bunnell, B.A., Casteilla, L., Dominici, M., Katz, A.J., March, K.L., Redl, H., Rubin, J.P., Yoshimura, K., and Gimble, J.M. (2013). Stromal cells from the adipose tissue-derived stromal vascular fraction and culture expanded adipose tissue-derived stromal/stem cells: a joint statement of the International Federation for Adipose Therapeutics and Science (IFATS) and the International Society for Cellular Therapy (ISCT). *Cytotherapy* 15, 641–648.
32. Janowski, M., Kuzma-Kozakiewicz, M., Binder, D., Habisch, H.J., Habich, A., Lukomska, B., Domanska-Janik, K., Ludolph, A.C., and Storch, A. (2008). Neurotransplantation in mice: the condrille-like position ensures minimal cell leakage and widespread distribution of cells transplanted into the cisterna magna. *Neurosci. Lett.* 430, 169–174.
33. Mead, R.J., Bennett, E.J., Kennerley, A.J., Sharp, P., Sunyach, C., Kasher, P., Berwick, J., Pettmann, B., Battaglia, G., Azzouz, M., et al. (2011). Optimised and rapid pre-clinical screening in the SOD1(G93A) transgenic mouse model of amyotrophic lateral sclerosis (ALS). *PLoS ONE* 6, e23244.
34. Tripathi, P., Rodriguez-Muela, N., Klim, J.R., de Boer, A.S., Agrawal, S., Sandoe, J., Lopes, C.S., Ogliairi, K.S., Williams, L.A., Shear, M., et al. (2017). Reactive Astrocytes Promote ALS-like Degeneration and Intracellular Protein Aggregation in Human Motor Neurons by Disrupting Autophagy through TGF- β 1. *Stem Cell Reports* 9, 667–680.
35. Wichterle, H., Lieberam, I., Porter, J.A., and Jessell, T.M. (2002). Directed differentiation of embryonic stem cells into motor neurons. *Cell* 110, 385–397.
36. Di Giorgio, F.P., Carrasco, M.A., Siao, M.C., Maniatis, T., and Eggan, K. (2007). Non-cell autonomous effect of glia on motor neurons in an embryonic stem cell-based ALS model. *Nat. Neurosci.* 10, 608–614.
37. Marconi, S., Castiglione, G., Turano, E., Bissolotti, G., Angiari, S., Farinazzo, A., Constantin, G., Bedogni, G., Bedogni, A., and Bonetti, B. (2012). Human adipose-derived mesenchymal stem cells systemically injected promote peripheral nerve regeneration in the mouse model of sciatic crush. *Tissue Eng. Part A* 18, 1264–1272.
38. Chen, H., Min, X.H., Wang, Q.Y., Leung, F.W., Shi, L., Zhou, Y., Yu, T., Wang, C.M., An, G., Sha, W.H., and Chen, Q.K. (2015). Pre-activation of mesenchymal stem cells with TNF- α , IL-1 β and nitric oxide enhances its paracrine effects on radiation-induced intestinal injury. *Sci. Rep.* 5, 8718.
39. Nicaise, C., Mitrecic, D., and Pochet, R. (2011). Brain and spinal cord affected by amyotrophic lateral sclerosis induce differential growth factors expression in rat mesenchymal and neural stem cells. *Neuropathol. Appl. Neurobiol.* 37, 179–188.
40. Sun, H., Bénardais, K., Stanslowsky, N., Thau-Habermann, N., Hensel, N., Huang, D., Claus, P., Dengler, R., Stangel, M., and Petri, S. (2013). Therapeutic potential of mesenchymal stromal cells and MSC conditioned medium in Amyotrophic Lateral Sclerosis (ALS)—in vitro evidence from primary motor neuron cultures, NSC-34 cells, astrocytes and microglia. *PLoS ONE* 8, e72926.
41. Endo, F., Komine, O., Fujimori-Tonou, N., Katsuno, M., Jin, S., Watanabe, S., Sobue, G., Dezawa, M., Wyss-Coray, T., and Yamanaka, K. (2015). Astrocyte-derived TGF- β 1 accelerates disease progression in ALS mice by interfering with the neuroprotective functions of microglia and T cells. *Cell Rep.* 11, 592–604.
42. Kia, A., McAvoy, K., Krishnamurthy, K., Trotti, D., and Pasinelli, P. (2018). Astrocytes expressing ALS-linked mutant FUS induce motor neuron death through release of tumor necrosis factor- α . *Glia* 66, 1016–1033.
43. Varciana, A., Myszczyńska, M.A., Castelli, L.M., O'Neill, B., Kim, Y., Talbot, J., Nyberg, S., Nyamali, I., Heath, P.R., Stopford, M.J., et al. (2019). Micro-RNAs secreted through astrocyte-derived extracellular vesicles cause neuronal network degeneration in C9orf72 ALS. *EBioMedicine* 40, 626–635.
44. Oh, K.W., Moon, C., Kim, H.Y., Oh, S.I., Park, J., Lee, J.H., Chang, I.Y., Kim, K.S., and Kim, S.H. (2015). Phase I trial of repeated intrathecal autologous bone marrow-derived mesenchymal stromal cells in amyotrophic lateral sclerosis. *Stem Cells Transl. Med.* 4, 590–597.
45. Oh, K.W., Noh, M.Y., Kwon, M.S., Kim, H.Y., Oh, S.I., Park, J., Kim, H.J., Ki, C.S., and Kim, S.H. (2018). Repeated Intrathecal Mesenchymal Stem Cells for Amyotrophic Lateral Sclerosis. *Ann. Neurol.* 84, 361–373.
46. Staff, N.P., Madigan, N.N., Morris, J., Jentoft, M., Sorenson, E.J., Butler, G., Gastineau, D., Dietz, A., and Windebank, A.J. (2016). Safety of intrathecal autologous adipose-derived mesenchymal stromal cells in patients with ALS. *Neurology* 87, 2230–2234.
47. Scott, S., Kranz, J.E., Cole, J., Lincecum, J.M., Thompson, K., Kelly, N., Bostrom, A., Theodoss, J., Al-Nakhala, B.M., Vieira, F.G., et al. (2008). Design, power, and interpretation of studies in the standard murine model of ALS. *Amyotroph. Lateral Scler.* 9, 4–15.
48. Fischer, L.R., Culver, D.G., Tennant, P., Davis, A.A., Wang, M., Castellano-Sanchez, A., Khan, J., Polak, M.A., and Glass, J.D. (2004). Amyotrophic lateral sclerosis is a distal axonopathy: evidence in mice and man. *Exp. Neurol.* 185, 232–240.
49. Brustle, D.A., Cutler, R.G., Telljohann, R.S., and Mattson, M.P. (2009). Decline in daily running distance presages disease onset in a mouse model of ALS. *Neuromolecular Med.* 11, 58–62.
50. Kasarskis, E.J., and Winslow, M. (1989). When did Lou Gehrig's personal illness begin? *Neurology* 39, 1243–1245.
51. Habisch, H.J., Janowski, M., Binder, D., Kuzma-Kozakiewicz, M., Widmann, A., Habich, A., Schwalenstöcker, B., Hermann, A., Brenner, R., Lukomska, B., et al. (2007). Intrathecal application of neuroectodermally converted stem cells into a mouse model of ALS: limited intraparenchymal migration and survival narrows therapeutic effects. *J. Neural. Transm. (Vienna)* 114, 1395–1406.
52. Noh, M.Y., Cho, K.A., Kim, H., Kim, S.-M., and Kim, S.H. (2014). Erythropoietin modulates the immune-inflammatory response of a SOD1(G93A) transgenic mouse model of amyotrophic lateral sclerosis (ALS). *Neurosci. Lett.* 574, 53–58.
53. Rajan, T.S., Diomedea, F., Bramanti, P., Trubiani, O., and Mazzon, E. (2017). Conditioned medium from human gingival mesenchymal stem cells protects

- motor-neuron-like NSC-34 cells against scratch-injury-induced cell death. *Int. J. Immunopathol. Pharmacol.* *30*, 383–394.
54. Ooi, Y.Y., Dheen, S.T., and Tay, S.S. (2015). Paracrine effects of mesenchymal stem cells-conditioned medium on microglial cytokines expression and nitric oxide production. *Neuroimmunomodulation* *22*, 233–242.
 55. Noh, M.Y., Lim, S.M., Oh, K.W., Cho, K.A., Park, J., Kim, K.S., Lee, S.J., Kwon, M.S., and Kim, S.H. (2016). Mesenchymal Stem Cells Modulate the Functional Properties of Microglia via TGF- β Secretion. *Stem Cells Transl. Med.* *5*, 1538–1549.
 56. Kwon, M.S., Noh, M.Y., Oh, K.W., Cho, K.A., Kang, B.Y., Kim, K.S., Kim, Y.S., and Kim, S.H. (2014). The immunomodulatory effects of human mesenchymal stem cells on peripheral blood mononuclear cells in ALS patients. *J. Neurochem.* *131*, 206–218.
 57. Lladó, J., Tolosa, L., and Olmos, G. (2013). Cellular and molecular mechanisms involved in the neuroprotective effects of VEGF on motoneurons. *Front. Cell. Neurosci.* *7*, 181.
 58. Gu, R., Hou, X., Pang, R., Li, L., Chen, F., Geng, J., Xu, Y., and Zhang, C. (2010). Human adipose-derived stem cells enhance the glutamate uptake function of GLT1 in SOD1(G93A)-bearing astrocytes. *Biochem. Biophys. Res. Commun.* *393*, 481–486.
 59. Nadjar, A., Berton, O., Guo, S., Leneuve, P., Dovero, S., Diguët, E., Tison, F., Zhao, B., Holzenberger, M., and Bezard, E. (2009). IGF-1 signaling reduces neuro-inflammatory response and sensitivity of neurons to MPTP. *Neurobiol. Aging* *30*, 2021–2030.
 60. Bellini, M.J., Hereñú, C.B., Goya, R.G., and Garcia-Segura, L.M. (2011). Insulin-like growth factor-I gene delivery to astrocytes reduces their inflammatory response to lipopolysaccharide. *J. Neuroinflammation* *8*, 21.
 61. Labandeira-Garcia, J.L., Costa-Besada, M.A., Labandeira, C.M., Villar-Cheda, B., and Rodríguez-Perez, A.I. (2017). Insulin-Like Growth Factor-1 and Neuroinflammation. *Front. Aging Neurosci.* *9*, 365.
 62. Vincent, A.M., Mobley, B.C., Hiller, A., and Feldman, E.L. (2004). IGF-I prevents glutamate-induced motor neuron programmed cell death. *Neurobiol. Dis.* *16*, 407–416.
 63. Bogaert, E., Van Damme, P., Van Den Bosch, L., and Robberecht, W. (2006). Vascular endothelial growth factor in amyotrophic lateral sclerosis and other neurodegenerative diseases. *Muscle Nerve* *34*, 391–405.
 64. Uccelli, A., Milanese, M., Principato, M.C., Morando, S., Bonifacino, T., Vergani, L., Giunti, D., Voci, A., Carminati, E., Giribaldi, F., et al. (2012). Intravenous mesenchymal stem cells improve survival and motor function in experimental amyotrophic lateral sclerosis. *Mol. Med.* *18*, 794–804.
 65. Keifer, O.P., Jr., O'Connor, D.M., and Boulis, N.M. (2014). Gene and protein therapies utilizing VEGF for ALS. *Pharmacol. Ther.* *141*, 261–271.
 66. Gouel, F., Rolland, A.S., Devedjian, J.C., Burnouf, T., and Devos, D. (2019). Past and Future of Neurotrophic Growth Factors Therapies in ALS: From Single Neurotrophic Growth Factor to Stem Cells and Human Platelet Lysates. *Front. Neurol.* *10*, 835.
 67. Bonafede, R., Scambi, I., Peroni, D., Potrich, V., Boschi, F., Benati, D., Bonetti, B., and Mariotti, R. (2016). Exosome derived from murine adipose-derived stromal cells: Neuroprotective effect on in vitro model of amyotrophic lateral sclerosis. *Exp. Cell Res.* *340*, 150–158.
 68. Lee, M., Ban, J.J., Kim, K.Y., Jeon, G.S., Im, W., Sung, J.J., and Kim, M. (2016). Adipose-derived stem cell exosomes alleviate pathology of amyotrophic lateral sclerosis in vitro. *Biochem. Biophys. Res. Commun.* *479*, 434–439.
 69. Anderson, P., Carrillo-Gálvez, A.B., and Martín, F. (2015). Isolation of Murine Adipose Tissue-derived Mesenchymal Stromal Cells (mASCs) and the Analysis of Their Proliferation in vitro. *Bio Protoc.* *5*, e1642.
 70. Guasti, L., Prasongchean, W., Kleftouris, G., Mukherjee, S., Thrasher, A.J., Bulstrode, N.W., and Ferretti, P. (2012). High plasticity of pediatric adipose tissue-derived stem cells: too much for selective skeletogenic differentiation? *Stem Cells Transl. Med.* *1*, 384–395.
 71. Peister, A., Mellad, J.A., Larson, B.L., Hall, B.M., Gibson, L.F., and Prockop, D.J. (2004). Adult stem cells from bone marrow (MSCs) isolated from different strains of inbred mice vary in surface epitopes, rates of proliferation, and differentiation potential. *Blood* *103*, 1662–1668.
 72. Wang, Q., Steigelman, M.B., Walker, J.A., Chen, S., Hornsby, P.J., Bohnenblust, M.E., and Wang, H.T. (2009). In vitro osteogenic differentiation of adipose stem cells after lentiviral transduction with green fluorescent protein. *J. Craniofac. Surg.* *20*, 2193–2199.
 73. Guasti, L., Vagaska, B., Bulstrode, N.W., Seifalian, A.M., and Ferretti, P. (2014). Chondrogenic differentiation of adipose tissue-derived stem cells within nanocaged POSS-PCU scaffolds: a new tool for nanomedicine. *Nanomedicine (Lond.)* *10*, 279–289.
 74. Ludolph, A.C., Bendotti, C., Blaugrund, E., Chio, A., Greensmith, L., Loeffler, J.P., Mead, R., Niessen, H.G., Petri, S., Pradat, P.F., et al. (2010). Guidelines for preclinical animal research in ALS/MND: A consensus meeting. *Amyotroph. Lateral Scler.* *11*, 38–45.
 75. Faul, F., Erdfelder, E., Buchner, A., and Lang, A.G. (2009). Statistical power analyses using G*Power 3.1: tests for correlation and regression analyses. *Behav. Res. Methods* *41*, 1149–1160.
 76. Russell, W.M.S., and Burch, R.L. (1959). *The Principles of Humane Experimental Technique* (Methuen; reprinted by UFAW).
 77. Iannitti, T., Scarrott, J.M., Likhite, S., Coldicott, I.R.P., Lewis, K.E., Heath, P.R., Higginbottom, A., Myszczyńska, M.A., Milo, M., Hautbergue, G.M., et al. (2018). Translating SOD1 Gene Silencing toward the Clinic: A Highly Efficacious, Off-Target-free, and Biomarker-Supported Strategy for fALS. *Mol. Ther. Nucleic Acids* *12*, 75–88.
 78. Frakes, A.E., Ferraiuolo, L., Haidet-Phillips, A.M., Schmelzer, L., Braun, L., Miranda, C.J., Ladner, K.J., Bevan, A.K., Foust, K.D., Godbout, J.P., et al. (2014). Microglia induce motor neuron death via the classical NF- κ B pathway in amyotrophic lateral sclerosis. *Neuron* *81*, 1009–1023.
 79. Saura, J., Tusell, J.M., and Serratos, J. (2003). High-yield isolation of murine microglia by mild trypsinization. *Glia* *44*, 183–189.
 80. Stopford, M.J., Allen, S.P., and Ferraiuolo, L. (2019). A High-throughput and Pathophysiologically Relevant Astrocyte-motor Neuron Co-culture Assay for Amyotrophic Lateral Sclerosis Therapeutic Discovery. *Bio. Protoc.* *9*, e3353.
 81. Allen, S.P., Hall, B., Castelli, L.M., Francis, L., Woof, R., Siskos, A.P., Kouloura, E., Gray, E., Thompson, A.G., Talbot, K., et al. (2019). Astrocyte adenosine deaminase loss increases motor neuron toxicity in amyotrophic lateral sclerosis. *Brain* *142*, 586–605.